

Targeting the Bitter Taste Receptors to Modulate the Bitter Aftertaste of Stevia for Diabetic Patients.



By

Maria Hassan Khan

(Registration No: 00000401350)

Department of Sciences

School of Interdisciplinary Engineering & Sciences (SINES)

National University of Sciences & Technology (NUST)

Islamabad, Pakistan

August 2024

Targeting the Bitter Taste Receptors to Modulate the Bitter Aftertaste of Stevia for Diabetic Patients.



By

Maria Hassan Khan

(Registration No: 00000401350)

A thesis submitted to the National University of Sciences & Technology, Islamabad,

In partial fulfillment of the requirements for the degree of

**Master of Science in
Bioinformatics**

Supervisor: Dr. Ishrat Jabeen

School of Interdisciplinary Engineering & Sciences (SINES)

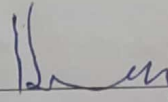
National University of Sciences & Technology (NUST)

Islamabad, Pakistan

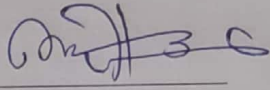
August 2024

THESIS ACCEPTANCE CERTIFICATE

Certified that final copy of MS/MPhil thesis written by Ms Maria Hassan Khan Registration No. 00000401350 of SINES has been vetted by undersigned, found complete in all aspects as per NUST Statutes/Regulations, is free of plagiarism, errors, and mistakes and is accepted as partial fulfillment for award of MS/MPhil degree. It is further certified that necessary amendments as pointed out by GEC members of the scholar have also been incorporated in the said thesis.


Signature with stamp: 
Name of Supervisor: **Prof. Dr. Ishrat Jabeen**
Date: 29-08-2024

DR. ISHRAT JABEEN
Professor
School of Interdisciplinary
Engineering & Sciences
NUST Sector H-12 Islamabad

Signature of HoD with stamp: 
Date: 29/08/2024

Dr. Mian Ilyas Ahmad
HcD Engineering
Professor
SINES - NUST, Sector H-12
Islamabad

Countersign by

Signature (Dean/Principal): 
Date: 29/08/2024

AUTHOR'S DECLARATION

I Maria Hassan Khan hereby state that my MS thesis titled Targeting the Bitter Taste Receptors to Modulate the Bitter Aftertaste of Stevia for diabetic patients is my work and has not been submitted previously by me for taking any degree from the National University of Sciences and Technology, Islamabad, or anywhere else in the country/ world.

At any time if my statement is found to be incorrect even after I graduate, the university has the right to withdraw my MS degree.

Name of Student: Maria Hassan Khan

Date: July 8, 2024

PLAGIARISM UNDERTAKING

I solemnly declare that the research work presented in the thesis titled “**Targeting the Bitter Taste Receptors to Modulate the Bitter Aftertaste of Stevia for Diabetic Patients**” is solely my research work with no significant contribution from any other person. Small contribution/help wherever taken has been duly acknowledged and that complete thesis has been written by me.

I understand the zero-tolerance policy of the HEC and the National University of Sciences and Technology (NUST), Islamabad towards plagiarism. Therefore, I as an author of the above-titled thesis declare that no portion of my thesis has been plagiarized and any material used as reference is properly referred to/cited.

I undertake that if I am found guilty of any formal plagiarism in the above-titled thesis even after the award of the MS degree, the University reserves the right to withdraw/revoke my MS degree and that HEC and NUST, Islamabad have the right to publish my name on the HEC/University website on which names of students are placed who submitted plagiarized thesis.

Student Signature: _____

Name: Maria Hassan Khan

DEDICATION

I dedicate this thesis to my beloved parents and siblings, especially my brother (Ahmed Hassan Khan) whose prayers, love, encouragement, and endless support made my success possible, and to my teachers, whose help and guidance helped me throughout my academic journey.

Acknowledgement

First of all, I am deeply grateful to **Allah Almighty**, whose countless blessings and guidance have brought me to this point in my educational journey. None of this would have been possible without His grace and mercy.

I want to express my sincere gratitude to my supervisor **Dr. Ishrat Jabeen**. Your guidance, patience, and invaluable guidance have been of great help in completing this thesis. Your encouragement and belief in my abilities have helped me through the challenges of this research.

I am deeply thankful to my GEC members, **Dr. Masood Ur Rahman Kayani** and **Dr. Uzma Habib**, for their insightful guidance and constructive feedback. Your expertise and advice have helped shape this thesis and guide me through the research process.

I would like to express my deepest gratitude to **my Parents**, whose unwavering support and endless sacrifices have been my pillars of strength. His encouragement and belief in me have always been the driving force behind my achievements. I am also extremely grateful to my brother **Ahmed Hassan Khan** for his constant encouragement and for always being with me. My friends **Zill-e-Noor and Fatima Nawazish, Maham Naveed, Ayesha Maqbool**, and **Umme Habiba** deserve special recognition for their continuous support and company during this journey. Your support and positivity have given me lots of comfort and inspiration. I also want to express my sincere gratitude to my lab fellow **Minahil Tariq**, for her support. Special thanks to my partner **Younieb Khan** whose support and encouragement helped me to complete my thesis. Your encouragement made a significant difference during this difficult journey.

Table of Contents

Acknowledgement	9
Abstract	17
Chapter 1: Introduction	18
1.1 Diabetes Mellitus	18
1.2 Sugars as a Regular Sweetener	18
1.3 Stevia Rebaudiana – A Natural Sugar Alternative	19
.....	20
1.4 Limitations on the Use of Steviol Glycosides	20
1.5 Human Bitter Taste Receptors (GPCRS)	21
1.6 Inhibitors for TAS2Rs	21
1.7 Need of the Study	21
1.8 Objective	22
Chapter 2: Literature Review	23
2.1 Impact of Sugar Consumption and Production	23
2.2 Sugar Consumption and its Long-Term Effects	24
2.3 Space for Natural Sweetener	25
2.4 Plant-Based Sweetener	25
2.5 Stevia and Its Constituents	26
2.6 Ecology	27
2.7 Components of Stevia	27
2.8 Commercial Value of Stevia	27

2.9 The Bitter Aftertaste of Stevia	28
2.10 Taste Receptors of Humans	28
2.11 TAS2R GPCRs- Bitter Taste Receptors	29
2.12 TAS2Rs Involved in the Perception of Steviol Glycosides	30
2.13 Bitter Taste Receptor and Effect of TAS2R Antagonist	30
2.14 Inhibitors TAS2R4.....	31
2.15 Inhibitors TAS2R14.....	32
Chapter 3: Materials and Method.....	33
3. Protein Structure.....	33
3.1 Taste Receptor Type 2 Member 4 (TAS2R4)	33
3.2 Homology Modeling	34
3.3 Structure Evaluation.....	35
3.4 Taste Receptor 2 Type 14 (TAS2R14).....	35
3.4.1 TAS2R14 Structure Preparation	35
3.4.2 Loop Modeling and Structure Refinement.....	36
3.5 Protein Dynamic Simulations of TAS2R4.....	36
3.6 Protein Dynamic Simulation of Loop Modeled Structure of TAS2R14	37
3.7 Collection of Data for Ligands and their Preprocessing for Docking.	38
3.8 Ligands Preparation for Docking.....	38
3.9 Protein Preparation of TAS2R14 and TAS2R4.....	38
3.10 Molecular Docking	39
3.10.1 Pharmacophore Model	41

3.10.2 Molecular Docking for TAS2R4 Blockers	45
3.11 Molecular Dynamic Simulations (MD)	46
4.1 Homology Modelling TAS2R4.....	48
4.2 Loop Modelling of TAS2R14	50
4.3 Molecular Dynamic Simulation Analysis of TAS2R4.....	52
4.5 Molecular Dynamic Simulations of Loop Model TAS2R14.....	53
4.6 Molecular Docking TAS2R4 and TAS2R14 Results.....	55
4.7 Results of Pharmacophore Modeling.....	61
4.8 Molecular Docking TAS2R4 Blockers Results.....	63
4.8.1 Molecular Interaction.....	64
4.9 Molecular Dynamic Simulations (MD) of Complexes Results.....	70
Chapter 5: Conclusion and Future Perspective	75
References.....	77

Table of Figures

Figure 1.1: Stevia Rebaudiana Bertuni plant and leaf extract powder	20
Figure 3.1: Schematic Illustration of Overall Methodology	33
Figure 3.2: The figure shows the features on which the pharmacophore model was built.....	42
Figure 3.3: Workflow for Molecular Dynamic Simulation	47
Figure 4.1: Figure shows the template (7XP4) taken for TAS2R4.....	48
Figure 4.2: Sequence alignment of (TAS2R4) and (7XP4) Contains.....	49
Figure 4.3: Best predicted structure model of TAS2R4 based on their highest score	49
Figure 4.4: Shows the 8VY7 CryoEM structure of Gi-coupled TAS2R14 with cholesterol and an intracellular tastant	50
Figure 4.5: It shows the TAS2R14 structure	51
Figure 4.6: It shows the Loop model of TAS2R14 after loop modeling.	51
Figure 4.7: RMSD profile of TAS2R4 protein during MD simulations at 100ns	52
Figure 4.8: Root Mean Square Fluctuation (RMSF) plot for TAS2R4.	53
Figure 4.9: RMSD profile of TAS2R14 protein during MD simulations at 100ns	54
Figure 4.10: Root Mean Square Fluctuation (RMSF) plot for TAS2R14.	55
Figure 4.11: The red color shows TAS2R4 structure and blue color shows 7XP4 structure are perfectly superimposed.	56
Figure 4.12: A) Ramachandran plot for the first frame of TAS2R4 Structure	57
Figure 4.12: B) Ramachandran plot for the final frame of TAS2R4 Structure.....	58
Figure 4.13: A) Ramachandran plot for the first frame of TAS2R14 Structure	59
Figure 4.13: B) Ramachandran plot for the last frame of TAS2R14 Structure	60

Figure 4.14: A correlation graph for docking score (Gold score) and PIC50 values of TAS2R4.	60
Figure 4.15: A correlation graph for docking score (Gold score) and PIC50 values of TAS2R4.	61
Figure 4.16: A correlation graph for docking score (Gold score) and PIC50 values of TAS2R4 Blockers data.....	64
Figure 4.17: A) 2D Interaction Pattern of BCML Ligand and TAS2R4 Protein	65
Figure 4.17: B) 3D interactions of ligand BCML with Protein TAS2R14	66
Figure 4.18: A) 2D Interaction pattern of GABA Ligand and TAS2R4 protein	67
Figure 4.18: B) GABA ligand and protein TAS2R14 3D interactions	68
Figure 4.19: A) and B): 2D and 3D interaction pattern of GVI3727 ligand and TAS2R4 protein	69
Figure 4.20: B) MD simulation of highly active, least active, and moderate compounds of BCML ligand complex. It explains RMSD profile of BCML ligand complex during simulations at 100ns The RMSD (Root Mean Square Deviation) graph for the BCML protein and ligand complex shows the stability and conformational changes of both protein and ligand over a simulation time of 100 nanoseconds. The protein RMSD (blue line) initially increases and stabilizes around 3.0 to 4.0 Å, indicating that the protein reaches a relatively stable conformation after initial equilibrium. The ligand RMSD (red line) follows a similar trend, stabilizing around 2.5 to 3.5 Å, suggesting that the ligand remains permanently bound within the binding site while allowing some flexibility in the protein conformation and allowing adjustment. Overall, the graph indicates stable interactions between protein and ligand throughout the simulation	71
Figure 4.20: A) Shows protein-ligand contact after MD Simulation at 100ns	70
Figure 4.21: A) Shows protein-ligand contact after MD Simulation at 100ns	72

Figure 4.21: B) MD simulation of highly active, least active, and moderate compounds of GABA ligand complex. It explains RMSD profile of GABA ligand complex during simulations at 100ns. RMSD graph for GABA protein and ligand complex showing stability and conformational changes over a 100-nanosecond simulation period. The protein RMSD (blue line) shows an initial increase and stabilizes from about 3.5 to 4.8 Å, indicating that the protein acquires a stable conformation. The ligand RMSD (red line) follows a similar trend, stabilizing around 3.0 to 4.5 Å, suggesting that the ligand remains permanently bound within the binding site with some flexibility. Overall, the graph indicates stable interactions between the GABA protein and the ligand throughout the simulation 73

Figure 4.22: A) MD simulation of highly active, least active, and moderate compounds of GIV3727 ligand complex. It explains RMSD graph for GIV3727 protein and ligand complex showing stability and conformational changes over a 100 nanosecond simulation period. The protein RMSD (blue line) stabilizes from about 3.5 to 4.8 Å, indicating that the protein adopts a stable conformation. The ligand RMSD (red line) shows large fluctuations, which stabilize around 5.0 to 8.0 Å, indicating that when the ligand is bound, it exhibits significant flexibility and motion within the binding site. Is. Overall, the graph indicates that the protein-ligand complex maintains a stable interaction, with the ligand exhibiting significant changes. B) Protein-ligand contact after MD simulation of 100ns..... 74

Figure 4.22: B) Shows protein-ligand contact after MD Simulation at 100ns..... 74

List of Tables

Table 2.1: Some examples of natural sweetening compounds.....	26
Table 3.1: This Table shows the distances measured between features.....	42
Table 3.2: Table shows statistical parameters and distance matrix for the	43
Table 3.3: Inhibitors of Bitter taste receptor TAS2R4	45

Abstract

The structural dynamics and interaction mechanisms of the TAS2R4 and TAS2R14 bitter taste receptors enhance the palatability of the natural, zero-calorie sweetener *Stevia Rebaudiana*. Despite the health benefits of stevia, its bitter taste, due to the activation of TAS2R4 and TAS2R14 receptors, limits its acceptance, especially in diabetics who need an effective sugar substitute. The problem statement focuses on improving stevia's bitter sensory profile to promote better dietary adherence. Several studies have contributed to identifying research gaps, including a limited understanding of the molecular interactions between steviol glycosides and human bitter taste receptors and a lack of comprehensive research on natural sweetener substitutes that address taste modulation at the molecular level. Herein, molecular modeling strategies were used to predict the 3D structure of TAS2R4 and the TAS2R14 structures which were further refined by loop modeling and energy minimization. Molecular docking studies identified key residues involved in ligand binding, with BCML, GABA, and GIV3727 emerging as important blockers. Detailed 2D and 3D visualizations of these interactions provided deep insight into the molecular basis of taste receptor inhibition. MD simulations confirmed these results by showing stable protein-ligand interactions over 100 ns, with RMSD and RMSF analyses, highlighting the conformational stability and flexibility of the complexes. TAS2R14 was similarly analyzed, confirming stable binding interactions and identifying key residues through docking and MD simulations. The results showed that the identified inhibitors, BCML, GABA, and GIV3727, effectively interact with TAS2R4 and TAS2R14, stabilizing the receptor-ligand complex and possibly reducing the bitter taste of stevia. Ramachandran plots for both the initial and final frames of the simulations indicate a high percentage of residues in favored regions, ensuring the structural integrity of the models. A validated pharmacophore model and molecular docking identified five natural compounds as potential TAS2R4 and TAS2R14 modulators, showing key binding site similarities to known inhibitors. The study identified five natural compounds as promising modulators of TAS2R4 and TAS2R14, providing a strong basis for future therapeutic development targeting these receptors.

Chapter 1: Introduction

Diabetes mellitus is a disease is caused by insufficient insulin production or improper insulin consumption. According to the World Health Organization (WHO), there were 422 million diabetics worldwide in 2014, up from 108 million in 1980. In contrast to high-income countries, the prevalence of this disease is rising quickly in low- and middle-income countries. According to estimates, the disease directly caused 1.5 million people to die in 2019 and 2.2 million deaths in 2012 due to hyperglycemia (WHO, 2021). [1]

1.1 Diabetes Mellitus

Diabetes mellitus is a complex metabolic disease characterized by hyperglycemia, the disease's hallmark, which has different underlying causes in each of its subtypes. The autoimmune mediated loss of pancreatic beta cells results in the lack of insulin a crucial hormone that controls blood glucose causes type 1 diabetes. Insulin shortage or resistance to the effects of insulin may be present in other forms of diabetes. Type 1 diabetes accounts for about 5% of all cases, type 2 for 90%, and other subtypes for 5%. Over the past 30 years, diabetes has become more commonplace worldwide in terms of both incidence and prevalence. While an individual's tendency to T1DM and T2DM is a significant risk factor, the worldwide obesity epidemic and demographic shifts toward older people are probably other factors contributing to the rising prevalence of diabetes in society. Hypoglycemia can result from therapy with oral medications or insulin, and a breakdown of glucose directly causes metabolic problems such as diabetic ketoacidosis and hyperosmolar syndrome. Numerous tissues and organs, such as the kidneys, eyes, nerves, and cardiovascular system, are also affected by diabetes. Individuals with diabetes are more likely to die than people without the disease, mostly from cardiovascular conditions, at the same age.[2]

1.2 Sugars as a Regular Sweetener

Sugars are the most commonly used sweeteners around the globe. These artificial crystalline sugars are a part of daily diet across the globe whether in food, beverages and even some pharmaceutical products. According to statista.com, the market for stevia, a natural sweetener, is expected to be worth 405.6 million US dollars in 2024 and grow to over 739 million US dollars by 2034. Sugar market already is blooming and daily sugar intake across the globe is one the rise. Daily sugar intake mounts up to around 10% of our daily calorie intake that leads

a number of chronic and Non-Communicable Disease such as cardiovascular problems along with obesity and diabetes.[3].

According to the global stats issued by the World Health Organization (WHO), a total of around 40 and 41 million people die each year due to Non-Communicable Diseases (NCDs). Not only that, another WHO stats have shown that the number of diagnosed cases of diabetes and prediabetes has been on the rise since 1995. By 1995, a total of 180 million adults were affected by diabetes but by 2014, this number has gone up to 422 million. The ratio has been increased to 8.5% from 4.7% over the span of only 4-5 decades. (WHO, 2023).

As for Pakistan, diabetes has become a huge growing burden. The total number of diagnosed diabetes and prediabetes cases in Pakistan has went from between 40-60 million in 1995, all the way to 12-14 million individuals in 2011.[4]

Among all the regions in Pakistan, Sindh and Khyber Pakhtunkhwa having the highest number of diagnosed cases of diabetes. The leading factor of this outcome could be genetics, age, obesity and other underlying conditions.[5].With such an alarming rise, sugar intake should be monitored on an individual level. One of the most effective measure is to avoid these conditions is lowering the daily intake of these sugars. The best way to introduce a sugarless diet is to replace tabletop sugar with a non-caloric sweetener. A natural, a-caloric and vegan alternative to sucrose based sweeteners.[6]

1.3 Stevia Rebaudiana – A Natural Sugar Alternative

Stevia Rebaudiana Bertoni is a herbaceous, perennial herb that belongs to the family Asteraceae [7] and native to South America, especially northeastern Paraguay [8], which, due to its sweetening power, is known as "stevia" or "honey leaves" [9]. This plant grows naturally on the Amambian Mountain near the Mandy River (a narrow region between Brazil and Paraguay) and is currently cultivated in many parts of the world. This sweetening herb, which is unique to Argentina, Brazil, and Paraguay, is also referred to as sweet weed, sweet leaf, sweet herbs, and honey leaf. Stevia leaves have no calories and are sweeter than sugar. This plant yields steviol, a diterpenoid glycoside derivative that is safer to use as a sweetener than sucrose and sweeter than sucrose. Stevioside can be used as a substitute sweetener for those with hyperglycemia who are diabetic, obese, or otherwise unable to keep a rigorous diet. The plant has antibacterial, anti-inflammatory, hypotensive, antiseptic, diuretic, anti-fertility, and cardiogenic qualities in addition to its hypoglycemic effect. Additionally, it is effective in treating skin conditions like dermatitis, acne, eczema, etc. The people who have a

habit of drinking beverages and consuming sweetened food items, stevia leaves with enhanced phytoconstituents may be a good natural sweetener substitute[10].



Figure 1.1: Stevia Rebaudiana Bertuni plant and leaf extract powder.

According to The International Market Analysis Research and Consulting group (IMARC) the stevia global market is estimated to reach approximately 818 million US dollars by the year 2024. This indicates growing market for stevia as well as a market evolution and public perception towards a more sustainable, vegan, and organic sweetener. Along with the distinct taste, steviol glycosides impart several pharmaceutical benefits such as anti-hyperglycemic effects, antihypertensive effects, anticancer effects, antioxidant and antimicrobial activity, anti-tumor effect, effect on glucose absorption and on glucose synthesis, stimulates insulin secretion and effect on glucagon secretion.[11]

However, these glycosides are multifunctional as not they impart sweet taste; they also impart bitter aftertaste. Stevioside is the one glycoside that mounts up to 60 to 70% of the total glycosidic content of the stevia plant and alone is around 110-270 times sweeter than an average tabletop sugar such as sucrose. But along with the sweetness, stevioside brings about a bitter or licorice-like aftertaste. Rebaudioside A is the other glycoside that takes about 30-40% of the total glycoside content of stevia. It is also relatively 240-400 times more sweet than artificial tabletop sugar. However, it doesn't have as much of bitter aftertaste.[12]

1.4 Limitations on the Use of Steviol Glycosides

High potency sweeteners (HPSs) are substitutes that food and beverage manufacturers frequently utilize to reduce sugar intake and preserve sweetness levels in the diet. Although steviol glycosides are thought to be a more consumer-friendly option, some people find them to bitter aftertaste. Recently, bitterness and other undesirable qualities have been reduced with the discovery of flavor modulators [13]. Besides the pharmacological and sweetening

properties of steviol glycosides, food products and drinks sweetened with stevia sugars have an undesirable bitter aftertaste. It has been reported that the primary cause of this undesirable aftertaste is that these steviol glycosides attach to both the human tongue's bitter and sweet taste receptors. The G-protein coupled receptor (GPCR) family, which elicits the feeling of many taste sensations like bitter, sweet, salty, and amino-acid like umami flavor, includes human bitter taste receptors. More specifically, Type 1-TAS1R and Type 2-TAS2R are the two basic families into which these taste GPCRs are divided [14].

1.5 Human Bitter Taste Receptors (GPCRS)

The bitter, sweet, and umami compounds all activate taste receptor cells via G-protein coupled receptors. The bitter receptors come from the T2R family of receptors. In humans, bitter taste is sensed by 25 T2Rs. Bitter taste receptors (T2Rs) are chemosensory receptors with significant therapeutic potential. They are members of the superfamily of G protein-coupled receptors (GPCRs) [15]. From these twenty-five bitter receptors, TAS2R4 and TAS2R14 are found to be apparent receptors responsible for causing bitter aftertaste of steviol glycosides upon consumption which is also validated by the in-vitro studies performed in HEK 293 cell lines [16].

1.6 Inhibitors for TAS2Rs

Many in-vitro methods have been provided in previously indicated studies for reducing the harsh aftertaste of stevia. Recent heterologous expression investigations have indicated that certain chemical substances function as antagonists against human TAS2 receptors. These antagonists may function as hTAS2R suppressors when consumed with bitter substances. Additionally, it has been found that certain competitive inhibitors can block or inhibit the corresponding bitter taste receptors based on their IC₅₀ values. Some significant studies have proposed known inhibitors that can act as TAS2R4, and TAS2R14 blockers, thus facilitating comprehension of the mechanism of action of inhibitors and steviol glycosides for bitter taste receptors [17].

1.7 Need of the Study

To improve the bitter aftertaste of stevia and increase acceptance and compliance among diabetic patients many of whom require the use of sugar replacements to control their blood glucose levels it is essential to investigate how bitter taste receptors are modulated. Stevia's unpleasant bitterness may discourage long-term users, which would lower their quality of life and dietary satisfaction. Stevia may be made more palatable and enticing by minimizing the bitter aftertaste, which will benefit those with diabetes as well as those looking for healthier

sweeteners in general. This research has the potential to improve health outcomes and open up new business opportunities by advancing scientific innovation in taste perception, supporting the creation of food products with improved tastes, and endorsing natural sugar substitutes.

1.8 Objective

Diabetic patients experience a bitter aftertaste intake of stevia as a sugar substitute due to steviol glycoside-mediated activation of the bitter taste receptors.

This study aims to identify nature-driven inhibitors of bitter taste receptors thus, enhancing the taste of stevia for improved acceptance among individuals with diabetes.

1. Regulation mechanistic of bitter taste receptors.
2. Modulation of bitter taste receptor using natural antagonist along with stevia as sweetener.

Chapter 2: Literature Review

2.1 Impact of Sugar Consumption and Production

Sugar has always played a significant role as a basic tabletop sweetener in every household. Sugar has also played a major role as a sweetener in the preparation of many commercial food products since the beginning of times. Pakistan's estimated monthly consumption of sugar stands at 0.45 million tons. Consequently, a total of 5.4 million tons of sugar demand needs to be met to meet the local yearly demand. (Sugar Sector Study, 2021). Sugarcane propagation plays an important role in sugar production in Pakistan. Though not the sole parameter, sugarcane production still plays an important role in meeting the sugar demands annually.

According to data summarized by the Punjab Food Department, the sugar recovery rate has been around 10% and 11% in central and southern Punjab respectively in 2022 alone. (Pakistan, 2022). The daily sugar consumption in Pakistan is around 20kg per capita. With the increase in the population of Pakistan, it is obvious to conclude that the sugar intake rate has risen as well. During year 2022 and 2023, the sugar market in Pakistan was expected to rise at about 3.3% rate. A lot of the sugar efflux goes to the large corporations and business such as bakeries, beverages, ice-creams, candies etc. Surprisingly, a huge chunk of sugar is taken on by the beverage industry mounting up to a 1.2 million metric tons per annum. (Finance Division, GoP Islamabad, n.d.)

Non-communicable diseases or NCDs are the leading cause of death across the globe mounting up to around 41 million deaths a year, as stated by WHO. A number of reports have shown that the NCDs can usually be traced all the way back to the sugar consumption. As for global stats, around 71% if all deaths that occur globally are due to NCDs. Obesity, cardiovascular diseases, respiratory disorders and diabetes all are far behind NCDs in terms of death tolls. All 4 of the above mentioned diseases mount up to a total of 80% of the overall premature NCD deaths. Other than that, other chronic habits such as drinking and smoking increase the risk of demise via a NCD. According to WHO reports, 4 metabolic changes that increase the risk of NCD include Hypertension, Hyperlipidemia, Hyperglycemia and Obesity. (WHO, 2021)

There are four major metabolic changes caused by metabolic risk factors that increase the NCDs' risk including:

- High Blood Pressure
- Obesity/Overweight

- Hyperlipidemia (High level of fat found in blood)
- Hyperglycemia (High levels of glucose in blood)

Even though sugar is an essential part of everyday diet of a lot of people, the overall reputation of sugar remains controversial. Despite being an essential, sugar can be traced as the leading cause behind cardiovascular diseases.

Sugar discussed here is actually artificial, crystalline sugar, sugar naturally occurring in sweet fruits or vegetables or dairy is fine, healthy even. Plant based foods naturally contain essential amino acids, mineral and antioxidants. Dairy on the other hand is loaded with healthy proteins and rich in calcium. These natural produces take longer in the digestive system, which reports have shown actually reduces the risk of onset of cancer, diabetes and cardiovascular disorders. Excessive added sugar, as shelf-life extenders or flavorboosters, will bring about diabetes. [6].

2.2 Sugar Consumption and its Long-Term Effects

Added or artificial sugar is not to be associated only with sweetened food such as sweets, soft drinks etc. But excessive sugar is added to some of the less obvious foods as well such as bread, ketchup etc. This makes it difficult to monitor average calorie or sugar intake on a personal level. Excessive amounts of artificial sugars lead to hypertension as well as severe inflammation and eventually a chronic cardiovascular conditions. Unchecked and monitored sugar intake leads to unhealthy weight gain. Human body is designed to have an appetite control system. [18]

But sugar intake, essentially in liquid or beverage form leads to shutting the appetite control system off, leading to gradual rise in average calorie intake and of course, average weight gains too. The total number of diabetic and prediabetic diagnosed cases is on the rise since the last century. This rise can be observed across all regions of Pakistan. Sindh has seen the biggest rise among other regions and provinces whilst KPK has seen the lowest recorded cases among others. Though other than sugar intake, a number of other factors can be seen taken in to account with the higher risk of diabetes such as age, environmental factors as well hereditary factors, BMI, prior medical conditions. Out of the above mentioned factors, added sugar still remains the leading factor contributing to diabetes. [5]

2.3 Space for Natural Sweetener

With the increase in public understanding and trends to a healthier and vegan alternative to diet, companies are either changing or introducing a new line of sugar free foods via replacing aspartame based sugars with more concentrated and vegan based sweeteners. [6]

As of now, some of the most commonly used artificial sweeteners vigorously in food industries include cyclamate, aspartame, saccharin and acesulfame K. All of these sweeteners are high intensity, artificial and raise overall health concerns over regular intake of these sweeteners. Other than the obvious health concerns, these sweeteners also bitter, metallic or aromatic off-flavors as the quantity of these sweeteners is increased.

This off-putting taste is what makes these sweeteners limited. Above stated reasons are the main fuel in the ongoing search for a natural and a-caloric sweetener with minimum to none health concerns and no compromise on the taste.[12]

2.4 Plant-Based Sweetener

With the increase in public awareness and consciousness, what type of product is being consumed is under more scrutiny than ever. The general trend shift towards a healthier and organic diet is pushing the search for organic and vegan sweeteners.

Regardless of many options available in the market, the demand for non-caloric or low caloric sweeteners still remains. The conscious decision making regarding sweetener has increased the demand of natural sweeteners.

There are multiple compounds that are extracted from plants sources that have the potential to be used to as commercial sweeteners. Such as brazzein (extracted from *Pentadiplandra brazzeana*, an evergreen shrub), curculin (extracted from *Curculigo latifolia*), Erythritol (found in many sweet fruits and fermented food), steviol compounds (extracted from *Srebia rebaudiana*) etc. There are some natural sweetening compounds which are mention in the table below.[19].

Table 2.1: Some examples of natural sweetening compounds.

S.No.	Class of Natural sweetener	Examples	Plant source	Sweet principle	References
1.	Sweet proteins	Thaumatococin	<i>Thaumatococcus daniellii</i>	Thaumatococin I and II	[20]
2.	Sweet terpenoids	Triterpenoids	<i>Periandra dulcis mart.</i>	Glycyrrhizin, oleanane-type triterpenoid glycosides	[21]
3.	Sweet Polyketide	Dihydroisocoumarins	<i>Hydrangea macrophylla</i>	Phyllostachyin	(Kinghorn et al., 1986)
4.	Sweet terpenes	Steviol glycosides	<i>Stevia rebaudiana bertoni</i>	Stevioside, rebaudioside A	[22]

2.5 Stevia and Its Constituents

Stevia rebaudiana bertoni or more commonly known as just stevia is a perfect sugar alternative as it has all the aspects that are needed in terms of both public appeal and health-benefiting properties. Stevia is an edible, safe to consume, FDA approved, vegan and a low-calorie sweetener. The sweetening compounds, known as steviol glycosides, are non-interactive in nature, suggesting that they do not interact with other constituents in the same medium. This highlights the potential of stevia to be used as a commercial sweetener in beverages, candies, cakes, fondue etc. Unlike stevia, artificial sweeteners currently being used in food industries as of now, raises many health hazards namely obesity, bladder cancer and even brain tumor, all while being non-caloric. The FDA has certified the use of stevia as GRAS (Generally Regarded As safe), indicating that stevia or items produced from it are safe. In 2008, the Joint FAO/WHO Expert Committee on Food Additives (JECFA) established a suggested ADI of 4 mg/day for

stevia. Apart from the statements provided by the FDA and WHO, stevia has been a popular sweetener in Paraguay for over 1500 years. The population's very existence and overall health status serve as sufficient evidence that stevia is safe to eat and has no significant long-term health risks. [23]

A 2017 study that found steviol glycosides to be non-mutagenic, teratogenic, and even carcinogenic provides additional evidence in favor of stevia's safety claims. Steviol glycosides have no known toxicity. [24]

2.6 Ecology

Stevia is a perennial herbaceous plant that is native to Brazil and west Paraguay, respectively. It is a member of the Asteraceae family. It can be grown and is currently grown in China, India, Korea, Brazil, Thailand, and Central America. The optimal temperature range for stevia cultivation is between 40°C at night and 48°C during the day. Higher latitudes were shown to yield a higher percentage of sweet glycosides in the plants. An additional study by Hossain et al. (2017) revealed that stevia vegetative development decreased at temperatures below 20°. Additionally, when the day's duration is reduced to less than twelve hours. [25]

2.7 Components of Stevia

Glycosides are the components of stevia that have attracted the interest of scientists and researchers worldwide. The natural class of molecules called steviol glycosides is present in stevia plants, and it is these phytochemicals that are responsible for the plant's sweet flavor. Stevioside (3–10%), Rebaudioside A (13%), and Rebaudioside B, C, and D which are of greater significance. Other similar chemicals are Dlucoside A and Rebaudioside C (1-2%). A few lesser glycosides are flavonoid glycosides, cinnamic acids, coumarins, certain essential oils, and phenylpropanoids, in addition to the major sweet glycosides already mentioned. [26]

Stevia leaves also contain sweetening triterpenes, sterols, and esters in addition to sweetening glycosides. These sweetening chemicals, as well as our components of interest, rebaudioside A and stevioside, may be extracted from dried stevia leaves. Each of these substances is 200–350 times sweeter than typical artificial sugars. 5–10% of the stevioside that was extracted from dried leaves had a yield of 2–4% of rebaudioside A. (Verónica López-Carbón et al., 2019)

2.8 Commercial Value of Stevia

High-purity sweeteners, generated over US\$ 492 million in profit in 2018 and are expected to generate approximately US\$ 1.16 billion by 2026, making it a well-recognized industry

today.[28]The concept of sweetening food with stevia is not new at all. Currently now, you can easily find stevia leaves or leaf powder in any local market. Not just in households get these powders and leaves used as sweeteners for herbal drinks but also with industry. Larger companies like The Coca-Cola Company and The Pepsi Company currently offer a line of their standard beverages that contain stevia as a sweetener.

Stevia extraction is a safe method. Like all factories and businesses, the large-scale extraction and production of stevia-based products will generate waste in the years that follows. However, the leftovers from the stevia extracts would be utilized as fertilizer and/or an ingredient in animal feed. Because of this, the stevia business as a whole is significantly less harmful to the environment than any other. [29].

2.9 The Bitter Aftertaste of Stevia

Steviol glycosides have the unpleasant sensory attribute of leaving a bitter aftertaste in foods and beverages that contain them, in addition to their sweetening action. The fact that it holds binding affinity for both bitter and sweet taste receptors explains this aftertaste. GPCRs (G-protein coupled receptors), which induce the perception of different tastes like sweet, bitter, sour, and umami, are the taste receptors found in humans. The two families of human taste receptors are Type 1 (TAS1R), which is sweet, and Type 2 (TAS2R), which is bitter.

Study conducted by vijay Bhardwaj The ligands including both bitter and sweet taste receptors were used for molecular docking. Kamiya-8, one of the possible substitutes, was shown to have a limited affinity for bitter receptors and a good affinity for sweet taste based on binding energy analysis. More Kamiya-8 was chosen for molecular dynamics simulations to enhance the estimation of binding energy and verify Kamiya-8's binding strength with taste receptors. Additionally, the end-state free energies of molecules in a solvent were calculated using MM-PBSA, and it was discovered that Kamiya-8 has a double effect. [30]

2.10 Taste Receptors of Humans

The bitter, sweet, and umami compounds all activate taste receptor cells via G-protein coupled receptors. The bitter receptors come from the T2R family of receptors. In humans, bitter taste is sensed by 25 T2Rs, which are different from the accurate Class A GPCRs. Bitter taste receptors (T2Rs) are chemosensory receptors with significant therapeutic potential. They are members of the superfamily of G protein-coupled receptors (GPCRs). T2R4 and T2R14 are mainly involved in causing a bitter taste after taking stevia.[15]

The N-terminal region of sweet taste receptors has a calcium-binding site for Class C GPCRs, an orthosteric amino acid binding site, and substantial sequence homology with the periplasmic

binding protein of microorganisms. When TAS1R1 and TAS1R3 combine, monosodium glutamate, or umami flavor, is produced.[30]

2.11 TAS2R GPCRs- Bitter Taste Receptors

TAS2Rs, sometimes known as T2Rs, are members of the seven-transmembrane G protein-coupled receptor superfamily, which includes receptors for bitter taste. More than half of the medications now available target these receptors. According to conventional theory, T2Rs are found in the tongue's taste buds, where they first detect bitter flavors. On the other hand, increasing evidence suggests that T2Rs are extensively expressed throughout the body and that they use a variety of specialized mechanisms to mediate a range of contrasting tasks. The connection between T2Rs and their polymorphisms and human illnesses has also come to light. [31]

The activation mechanism of T2Rs. T2Rs has a unique signature sequence at the cytoplasmic end of the fifth trans membrane helix (TM5), a highly conserved LxxSL motif. An alanine scan mutagenesis of the ICL3 of T2R4 and characterize the functionality of 23 alanine mutants. Then this study identified the four mutants which are, H214A, Q216A, V234A, and M237A, and that exhibit constitutive activity. The H214A mutant showed very high constitutive activity over wild-type T2R4.[32]

The TAS2Rs in biological functions and diseases, no crystal structure is available to help understand the signal transduction mechanism or to help develop selective ligands as new therapeutic targets. They report the three-dimensional structure of the fully activated TAS2R4 human bitter taste receptor predicted using the GEnSeMBLE complete sampling method. TAS2R4 structure is coupled to the gustducin G protein and each of several agonists.[33]

Gene expression analyses in rodents demonstrated an essentially overlapping expression of TAS2R genes indicating a broad tuning, whereas functional *in vivo* analyses suggest a narrow tuning. The present study demonstrates the expression of all 25 human TAS2R genes in taste receptor cells of human circumvallate papillae. As shown by *in situ* hybridization experiments, the expression of hTAS2R genes differs in both the apparent level of expression and the number of taste receptor cells expressing these genes, suggesting a heterogeneous bitter taste receptor cell population. From the data of this study, it concluded that the human bitter taste receptor cells are tuned to detect a limited subset of bitter stimuli.[34]

Umami or taste receptors have been the focus of the majority of taste receptor research, both computational and experimental. There has been comparatively little published research on bitter taste receptors. The majority of the research discusses bitter taste receptors, which are

known to interact with a variety of agonists, including T2R14 and T2R16. Due to the orphanization of these bitter T2Rs (the ligands and function of which are still unknown) not enough research has been done.[35].

2.12 TAS2Rs Involved in the Perception of Steviol Glycosides

In order to identify the taste receptors responsible for neutralizing the bitter aftertaste of steviol glycosides, a study [16] was conducted in which 25 hTAS2Rs were briefly expressed in individual HEK293T $G\alpha_{16}$ gust44 cells. Different single nucleotide polymorphisms (SNP) in the human TAS2R genes can affect the function of the encoded receptors. Two receptors, hTAS2R4 and hTAS2R14, were shown to mediate the bitter aftertaste of steviol glycosides following a comprehensive screening of many human bitter taste receptors. The investigation also shows that, aside from rebaudioside D, they are sensitive to other steviol glycosides. This chemical may cause a bitter receptor response off-discovery limit because it elicited the lowest bitter taste in the previous sensory tests.

Both bitter taste receptors' positions differed in their potency against various steviol glycosides. For the most part, human TAS2R4 would be more susceptible to most test chemicals, with the greatest potency for rubusoside. The hTAS2R14 threshold values for the test compounds varied greatly, however they were all low for the steviol glycosides that include rhamnose, namely glucoside A, Rebaudioside C, and rubusoside. Numerous recent papers have provided a comprehensive overview of the agonist profiles of the two receptors. [36] [37]

While hTAS2R4 is triggered by a little amount of bitter tastants, its activation profile significantly resembles the widely tuned receptor hTAS2R14.[38].

2.13 Bitter Taste Receptor and Effect of TAS2R Antagonist

In the oral cavity, bitter taste receptors, or TAS2Rs, differentiate between different tastes. Antagonists of bitter GPCRs may be useful in suppressing the unpleasant taste and in facilitating the absorption of medications that have a bitter flavor. Recent research on heterologous expression has revealed that certain drugs function as antagonists against human TAS2Rs. In the oral cavity, taste molecules are distinguished by bitter taste receptors or TAS2Rs. Antagonists of bitter GPCRs may be useful in suppressing the unpleasant taste and in aiding the ingestion of medications with bitter tastes. Recent research on heterologous expression revealed that several drugs function as antagonists against human TAS2Rs. To find out whether these mixes work as bitter taste blockers, researchers [39] looked into the effects of a few human bitter receptor blockers on mice's behavioral lick reactions. In transient lick tests, adding the inhibitors did not affect lick reactions based on concentrations to bitter

compounds (quinine HCl, denatonium, and phenylthiourea). These results suggest that a few human TAS2R antagonists may effectively treat mice's bitter taste perception. However, only five bitter taste blockers or inhibitors are known to work against the twenty-five T2Rs, which are activated by a variety of bitter compounds with distinct structural variations.

2.14 Inhibitors TAS2R4

Studies that are reported the following inhibitors of TAS2R4 to be effective against activation of TAS2R4.

- **GABA and BCML**

In a study conducted by the University of Manitoba's Department of Oral Biology, calcium imaging assays led to the discovery of two amino acid derivatives as competitive inhibitors of quinine-activate T2R4: N α , N α -bis (carboxymethyl)-L-lysine (BCML) and Gamma-aminobutyric corrosive (GABA), with respective IC₅₀ values of 3.2 μ M and 59nM. Interestingly, pharmacological characterization using a constitutively active mutant of TAS2R4 reveals that BCML acts as an inverse antagonist on T2R4, whilst GABA acts as an agonist.[40]. The two novel bitter taste inhibitors have the same orthostatic location as the agonist quinine, as confirmed by site-directed mutagenesis. The interactions with BCML and GABA are significantly influenced by the signature residues of Ala-90 and Lys-270, respectively. The main report that described an inverse agonist and an endogenous antagonist of T2R was this one. The new bitter inhibitor may help in physiological research aimed at understanding the function of T2Rs in extra-oral organs.

- **Abscisic Acid (ABA)**

Another study from the Department of Oral Biology at the University of Manitoba found that plant hormones called abscisic acid (ABA), its precursor xanthoxin, and the catabolite phaseic acid can bind to T2R4 and either activate or inhibit it. Following molecular docking studies, calcium imaging functional assays demonstrated that ABA is an antagonist with an IC₅₀ value of 34.4 1.1 M.[40]

- **GIV3727**

GIV3727 was shown to inhibit both hTAS2R31 and hTAS2R43 in a study by [41]. This led to additional research to determine whether GIV3727 may inhibit other bitter receptors. Thus, its effects on calcium imaging were also examined utilizing a spectrum of transfected hTAS2Rs with known bitter agonists for 18 of the 25 hTAS2Rs, including TAS2R4. With a percentage

activation of 45.8% and a p value of 0.0067, the bitter agonist 10 mM colchicine activated TAS2R4 in the presence of GIV3727. [35].

2.15 Inhibitors TAS2R14

The TAS2R14 inhibitors that have been identified in the limited studies that have been published are given below.

- **GIV3727**

In addition to TAS2R4, GIV3727 has also demonstrated some inhibitory effects on TAS2R14. In the presence of GIV3727, 3 mM aristolochic acid triggered hTAS2R14 yields a percent activation of 94.3% with a p-value of 0.618.

- **6-Methoxyflavanones**

According to a study by, some flavanones have the ability to act as bitter receptor antagonists in addition to blocking the perception of bitter flavors. It has been observed that methyl flavanones, such as 6,3-dimethoxyflavanone, 6-methoxyflavanone, and 4-fluoro-6-methoxyflavanone, with IC₅₀ values in (μM) of 250000, 741000, and 500000, respectively, block the activation of hTAS2R14.[42]

Chapter 3: Materials and Method

In the current project various pharmacoinformatics including homology modeling, molecular docking, molecular dynamics simulation and Virtual Screening approaches were applied to probe the 2D and 3D structural features of the bitter taste receptors protein TAS2R4 and TAS2R14 to inhibit its bitter taste.

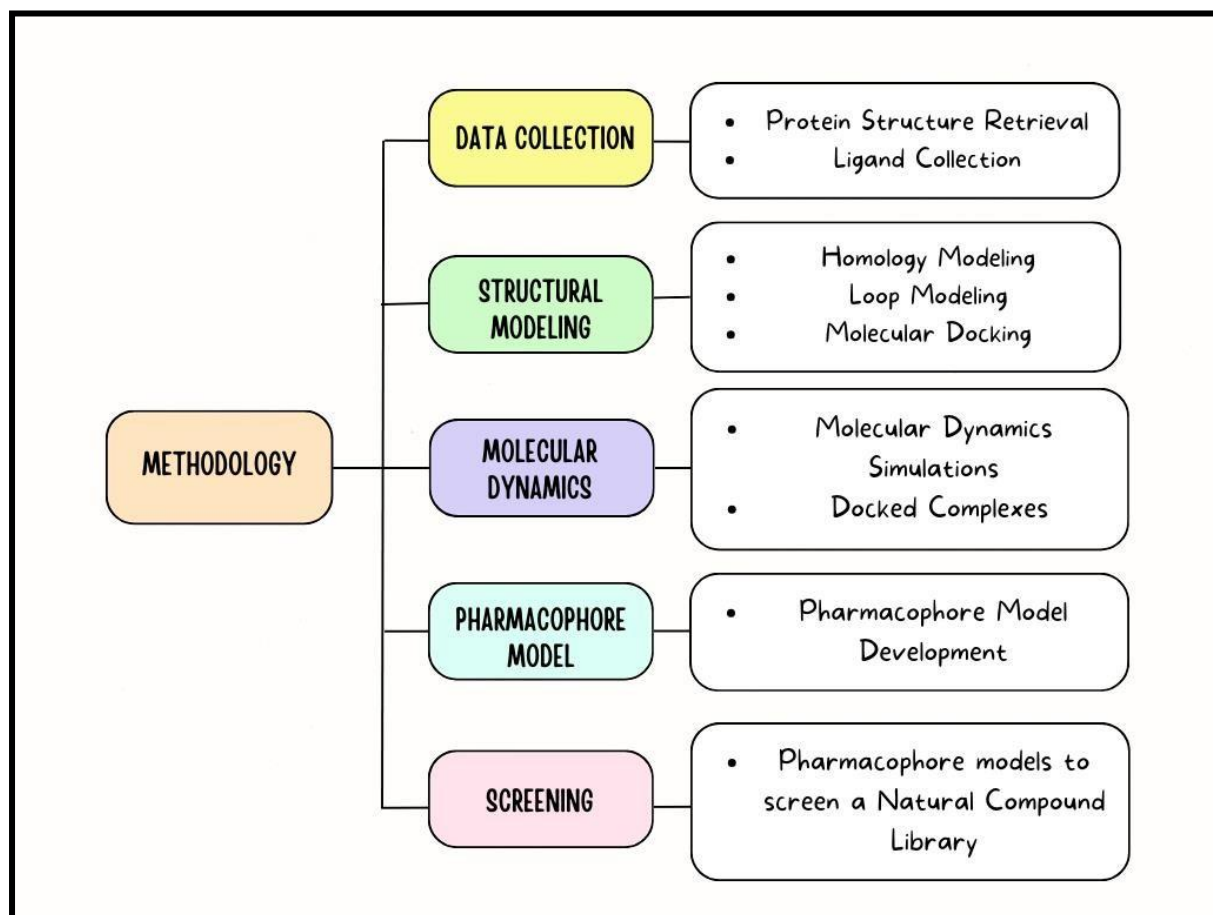


Figure 3.1: Schematic Illustration of Overall Methodology

3. Protein Structure

Bitter taste receptors TAS2R4 and TAS2R14 the X-ray crystallographic structure of TAS2R4 is not reported till date but the TAS2R14 X-ray crystallographic structure is reported so for the TAS2R4 therefore Homology Modeling has been performed using Modeller server.[43]

3.1 Taste Receptor Type 2 Member 4 (TAS2R4)

The structure of taste receptor type 2 member 4 is previously unknown. Only the alpha fold of TAS2R4 was found under the AF-Q9NYW5 -F1 identifier. The amino acid sequence of

TAS2R4 (accession no. Q9NYW5, entry name: TAS2R4_HUMAN) was retrieved from UniProt. [44]. The crystal structure of 7PX4 which is also a GPCR protein (PDB code: 7PX4, Entity 5, Chain E) [45] was selected as template due to maximum sequence similarity (29%).

3.2 Homology Modeling

Homology modelling also known as comparative modelling of protein that builds 3D structure for a target protein from its primary sequence and the related templates (homologs) of target protein. Modeller is the server used to predict the structure of TAS2R4 which works under homology modelling. MODELLER is a server that build 3D structure of protein on the basis of homology or comparative modelling. An alignment of sequence of protein to modelled with known homologs structures are provided by user and MODELLER calculates a model that contains all non-hydrogen atoms automatically. MODELLER can also perform modelling of loops in structure of protein by de novo method, optimization of many proteins structure models with respect to their defined objective function, protein sequences and/or structures multiple alignments, sequence database searching, clustering, and protein structures comparisons. Two approaches were used to build model using modeler.

First the addition of missing residues were done on the common PDB structure given by all three servers mentioned above. First save the python script under the name of protein PDB code with .py extension. By running the script on Modeller server, produces the sequence file with .seq extension. Make the alignment between the original structure (as the template) with gap characters corresponding to the missing residues and the full sequence while saving the file under the name of alignment with .ali extension. Run another python script of Loop Model class on modeller server. This script generates a model with all residues and refine the loop.

Second approach to use was Difficult modelling. This method is to Model a sequence on the basis of template. First, it is essential to convert the target TAS2R4 sequence into the PIR format readable by MODELLER (file "TAS2R4.ali") to search the structures related to target protein. After the search of structures, generate the multiple alignment using the templates. Save the python script containing the multiple alignments with the name of salign.py and run the script by the command salign () in Modeller server. In result, file was generated with PAP format containing the information on multiple sequence alignment score, no of matches, no of mismatches and gaps. Run another script of python to align query sequence to the template structures. For that task again use the salign () command to run the file under the name of `align2d_mult.py' file. Next, build the new model for the TAS2R4 target sequence on the basis

of alignment against the multiple templates using the python script under the name of 'model_mult.py' file.

3.3 Structure Evaluation

The evaluation of structures was conducted using model scores as the primary criterion. Five distinct models were generated during the study. Upon analysis, it was observed that the first model achieved the highest score among all. Therefore, the first model was selected for further analysis and application due to its highest score.

3.4 Taste Receptor 2 Type 14 (TAS2R14)

The cryoEM of Gi-coupled TAS2R14 with cholesterol and intracellular tastant is reported on PDB with 100% Sequence Similarity under the identifier **8VY7 (Homo sapiens)**.

3.4.1 TAS2R14 Structure Preparation

To understand the interactions of the TAS2R14 protein at a deeper level in a complex biological context, its crystal structure was first explored with a bound cholesterol, an intracellular tastant, and a ligand. The molecules of this protein-ligand, intracellular tastant, and cholesterol were carefully removed out from the structure using Chimera software (Pettersen et al., 2021). This would isolate the TAS2R14 protein and eliminate the interference of the bound molecules on an examination of the structural properties of the protein. Next, the modified structure of TAS2R14 was saved in PDB format for further structural and computational studies.

To this end, we considered chain E of the 637 amino acid TAS2R14 protein. The reason for choosing this particular chain is that it represents an entire sequence, which would be important in understanding the structural and functional features of TAS2R14. Therefore, the results are certain to generalize directly to human biology because *Homo sapiens* provided the protein sequence used in this study, possibly providing light on the function of the protein in taste perception in humans. To remove all structural characteristics related to TAS2R14, the ligand, intracellular tastant, and cholesterol have to be removed. The researchers sought to identify the basic structural elements of this protein that are important for its role as a taste receptor by focusing on its apo form or unbound form. To learn more about the function of the isolated TAS2R14 structure in taste perception and possible interactions with other tastants, docking experiments, and functional analysis will be conducted using the PDB file that was saved for the structure.

3.4.2 Loop Modeling and Structure Refinement

To provide an accurate and comprehensive structural model, our study used loop modeling to address missing residues in the TAS2R14 protein structure. Residues 159–173, 220–224, and 254–258 were found to be the missing loop regions. These regions thus played a critical role in the preservation of both structural integrity and functional characteristics of TAS2R14.

3.4.2.1 Software and Tools

ChimeraX, a state-of-the-art molecular visualization and modeling tool, was used for the loop modeling procedure. ChimeraX is the solution since it provides specific algorithms for loop prediction and refinement.

3.4.2.2 Procedure for Loop Modeling

It began with the import of the native crystal structure of TAS2R14 into ChimeraX, a state-of-the-art molecular visualization and modeling tool. Compounds bound to it, such as ligands, intracellular tastants, and cholesterol, were removed to focus on the protein alone. It then used ChimeraX with the sequence of TAS2R14, including the missing parts, to generate a tool for loop modeling. The program tries to predict accurate loop conformations given a sequence template and exact places for the residues that are missing. ChimeraX, by using its algorithms, modeled many such possible conformations from the given sequence in the structural context and generated five different models for missing loop regions.

For each of the generated models, the Z-DOPE score was calculated, which has been described as a statistical potential-based scoring function that evaluates predicted structures for precision and dependability by comparing them to native-like conformations. The Z-DOPE scores showed that the model with the highest value, that of -0.3, represented the most reliable and accurate representation of the missing loop region. These selected models were further refined to fit the complete TAS2R14 structure without steric conflicts and to maintain the realistic conformations. The full refined TAS2R14 structure with the integrated loop regions was stored in PDB format. This structure will be further employed in computational analyses, for instance, dynamic simulations or molecular docking.

3.5 Protein Dynamic Simulations of TAS2R4

In order to study the dynamic behavior and interactions of the TAS2R4 protein structure under physiological conditions, this work used molecular dynamics (MD) simulations. To minimize energy and minimize steric conflicts, the Amber 99 force field using MOE software [46] was used to optimize atomic locations in the basic structure of TAS2R4. The Schrödinger suite [47] was then used to get the minimized structure ready for MD simulations. The TAS2R4 structure

was preprocessed at a pH of 7.4 to simulate physiological pH values before MD simulations. The force field used in the simulations, optimal potentials for liquid simulations (OPLS3e), accurately depicts molecular interactions. In order to assess TAS2R4's interactions, it is essential to monitor the convergence of the heavy atom (HA) count with an RMSD tolerance of 0.3 Å to guarantee correct equilibration.

TAS2R4 was solvated by dissolving it in a solvent environment with the help of the SPC water model. An orthorhombic water box was generated to provide a buffer zone of 10 Å between the protein atoms and the box borders. The system was neutralized by adding 0.15 M of Na⁺ ions and Cl⁻ ions, which were carefully placed within a 5 Å radius. All MD runs were performed at a constant temperature of 303K to simulate physiology using the OPLS3e force field for energy calculations. As simulations were run for 100 ns, the dynamic behavior and interactions of TAS2R4 could be put through a very detailed analysis. The behavior and interactions of TAS2R4 in the course of MD simulation were analyzed using the Simulation Interaction Diagram, which is already built within the Desmond MD package. This approach provided a better view and understanding of protein-ligand interactions and the structural changes observed during the simulation.

The stability of the MD simulations is checked by plotting the RMSD of protein atoms and the RMSF of protein. It contributed to the complete understanding of the functional properties of TAS2R4 by shedding light on the structural stability and protein conformational dynamics during a simulation.

3.6 Protein Dynamic Simulation of Loop Modeled Structure of TAS2R14

Molecular dynamics simulations were conducted to observe the dynamic behavior of the loop-modeled TAS2R14 protein structure. Firstly, the structure was subjected to energy minimization using MOE, with the Amber 99 force field[46]. This would avoid steric conflicts or other unfavorable interactions. The reduced structure has been loaded into the MD simulations Schrödinger suite[47]. For considering biological conditions, TAS2R14 structure was preprocessed at a physiological pH of 7.4. To run the complex simulations, optimal potentials for liquid simulation force field OPLS3e was applied, that can accurately define molecular interactions. This RMSD of the HA count was set to be at 0.3 Å in order to have adequate equilibration so that we might determine the protein molecule interactions effectively.

After that, the structure was solved using the TIP3P water model, with the protein atoms and the box sides separated by a 10 Å buffer created by a cubic water box. Na⁺ and Cl⁻ ions were

introduced, recalculated, and concentrated to 0.15 M inside a 5 Å zone in order to neutralize the system. During the simulation, the temperature was kept at 303K, and energy calculations were carried out using the OPLS3e force field. This was further supported by 100 ns of MD simulations that provided an in-depth exploration of the behavior and interactions of the TAS2R14 protein with time.

Using the RMSD plots we investigate how behavior and protein interactions occur during the MD simulations. It provided an RMSD of the protein atom positions as a function of time, which showed the stability of the MD simulations, thus making the system stable with reliable insights into dynamic characteristics of TAS2R14.

3.7 Collection of Data for Ligands and their Preprocessing for Docking.

In the present study, an extended set of compounds of TAS2R14 inhibitors including 150 compounds has been retrieved from the ChEMBL database as shown in the Appendix. Each dataset item contained details such as IC₅₀ values, ChEMBL ID, and SMILES notation. Extensive preprocessing was done to guarantee the quality and docking fitness of the data. At the end, a fresh set of 119 unique compounds replaced the duplicate entries. This step was crucial in avoiding duplication and obtaining the accuracy of future analysis applications.

3.8 Ligands Preparation for Docking

The dataset was then pre-processed for molecular docking, and it contained 119 unique TAS2R14 inhibitors as shown in the appendix. Open Babel is the dynamic open source package of chemical informatics that was applied to process the smiles data of each compound. Thus, to ensure the correctness of covalent and electrostatic configurations, each molecule was added one extra hydrogen atom in this step. Moreover, Open Babel generated 2D and 3D coordinates of the compounds. Although 3D coordinates were necessary for an accurate positional alignment during the process of docking, 2D coordinates do make visualization and verification easier. This deep preprocessing ensured that the inhibitors were absolutely in their best form for the docking studies and thus predicted their interactions with TAS2R14 accurately.

3.9 Protein Preparation of TAS2R14 and TAS2R4

This was followed by the extraction of the last frame of the TAS2R14 and TAS2R4 protein structures in the Schrödinger software after the MD simulations. These structures were saved in the format of a CMS (Compressed System) file, a format that holds all the basic information of the system, such as coordinates for all atoms, simulation parameters, and system topology. The CMS file was loaded in the Molecular Operating Environment, MOE, to prepare protein structures for docking. A number of preparation actions were performed on the protein in MOE

to ensure that it would be in the best possible condition for docking. First of all, all heteroatoms and water molecules were removed from the structures. Since non-specific interactions could influence the results of docking, it was necessary to avoid this step.

Using Ramachandran plots, the quality and integrity of the protein structure were further confirmed. Residues in allowed and disallowed regions were found by analyzing these graphs which are made of the Swiss model[48] from the simulation's initial and last frames structures. This analysis made sure that during the simulation, the protein remained in a stable shape and that few residues fell into disallowed areas. Since it showed more stability, the final frame was chosen to serve as a basis for docking tests.

The protein structures were saved in the PDB (Protein Data Bank) format after they had been cleaned and processed. Because the PDB format can record atoms' 3D coordinates and make further research and docking easier, it is widely used in computational biology. The carefully developed protein structures were subsequently constructed for docking tests, ensuring precise and reliable predictions of interactions between the ligand and the TAS2R14 and TAS2R4 receptors.

3.10 Molecular Docking

Molecular docking was performed to identify the most probable binding conformations of modulators of selected biological targets using GOLD suite v.5.3.0. [49]. Both the loop-modeled TAS2R14 structure and the homology model of TAS2R4 were used in the molecular docking studies. GOLD software, which is known for its accuracy and reliability in ligand-protein interaction prediction, was utilized.

- **Binding Site Prediction for TAS2R14**

Through a thorough analysis of the literature, the binding site for TAS2R14 was found, which are Ile62, Phe76, Phe82, Leu85, Trp89, Ile179, Val180, Thr184, Ile187, Phe188, Phe243, Phe247, Ile262 assuring that the site chosen is important and has already been verified in studies[50]. However, binding site of proteins was selected around the 20A region that includes all the active residues identified from literature and the coordinates was selected as X: -2.7387, Y:-1.6913, Z:-4.993.

- **Binding Site Prediction for TAS2R4**

For TAS2R4, a comparative method was used to determine the binding position. Because of the two proteins' perfect superimposition and high degree of structural similarity, the structure of TAS2R4 was predicted using the 7PX4 entity 5 template. The structural alignment validated 7PX4's applicability as a template for the homology model TAS2R4. After then, the essential residues found in 7PX4's entity 5 binding site were precisely determined.[51]

The MOE (Molecular Operating Environment) Site Finder tool was used in order to further optimize the binding site residue selection for TAS2R4[46]. This method identified possible binding pockets and crucial residues involved in ligand binding by analyzing the homology model of TAS2R4. The residues were cross-checked detected in the 7PX4 entity 5 binding site with those discovered by the MOE Site Finder which are Leu159, Val160, Thr162, Arg163, Asn164, Phe168, Glu172, and Ser277. The residues chosen for the docking studies were the most precise ones, due to the dual-validation technique. However, binding site of proteins was selected around the 18A region that includes all the active residues identified from literature and the coordinates was selected as X: 1.8296, Y:-0.1408, Z: 12.561.

- **Poses Generation**

Both the ligand and protein were considered flexible by performing a total of 100 genetic algorithm runs per molecule using the gold score fitness function to enhance the conformational space. 10 poses were generated per compound. The best pose with the highest Dock score was selected for each molecule to explore the protein-ligand interactions inside the binding cavity of TAS2R4 and TAS2R14.

- **Correlation Analysis**

To predict the binding hypothesis and to reduce the conformational space, a strategies have been applied such correlation analysis between, PIC50 and docking score. For TAS2R4 and TAS2R14, the final pose for simulations was selected based on high correlation between PIC₅₀ and docking score.

After that, an investigation and comparison of protein-ligand interactions were done through docking simulations against the same dataset of compounds at TAS2R4 and TAS2R14. By doing so, one can directly compare the binding affinities, interaction patterns, and the docking scores for both proteins. This comparative study has, therefore, enabled us to understand how similar ligands interact with TAS2R4 and TAS2R14, hence making a vital contribution to the understanding of interaction processes and possible ligand interactions or selections toward these receptors.

3.10.1 Pharmacophore Model

It involved a complex process of modeling and analysis for ligand-protein interactions. First, the ligands were docked with the target protein using advanced molecular docking software that created ten different poses for each of the ligands. From these poses, the best one for every ligand was selected based on several factors, especially docking scores and binding interactions that met the idea of the most promising conformations being short-listed for further investigation.

Out of the rigorous dataset of 119 compounds, 35 compounds were filtered for detailed analysis. This thread creates a balanced dataset between active and inactive compounds, which is essential in developing a model that will be robust and predictive. Such a process used in this could also include careful classification of the active status of compounds into activity classes and validation of the dataset for its accuracy and reliability.

- **Classification of Data**

From the total dataset of 35 compounds, 17 were selected as actives and 18 as inactive. For detailed analysis. This selection is done to create a balanced dataset of active and inactive compounds, which is vital during the building process for a robust and predictive model. This is a process whereby compounds' activity status was carefully classified and validated to guarantee the accuracy and reliability of the dataset.

- **Model Building**

The pharmacophore model was then generated in the[52] based on docking confirmation. The reason for developing a pharmacophore model based on confirmation from docking was to make use of the very fine and specific details of binding interactions observed during the process of docking. It provides information on the spatial arrangement and patterns of interactions with which ligands bind to a target protein binding site. The pharmacophore model succeeded in capturing key features as shown in the figure below and interactions from top-docking poses, thereby contributing to the binding affinity and activity of ligands.

This approach ensures that only realistic and relevant conformations are included in the pharmacophore model so that it can deliver higher predictive accuracy for the identification of new potential active compounds. This provided a reliable basis for the docking conformations to reflect the real binding environment and interactions within the target protein.

Thereafter, the constructed pharmacophore model was much more accurate, but at the same time, its ability to distinguish active from inactive compounds was guaranteed. This study has thus developed a pharmacophore model that will be very useful for VS and drug discovery, based on the validation of docking. This technique provides a framework for filtering compounds of interest for further experimental validation.

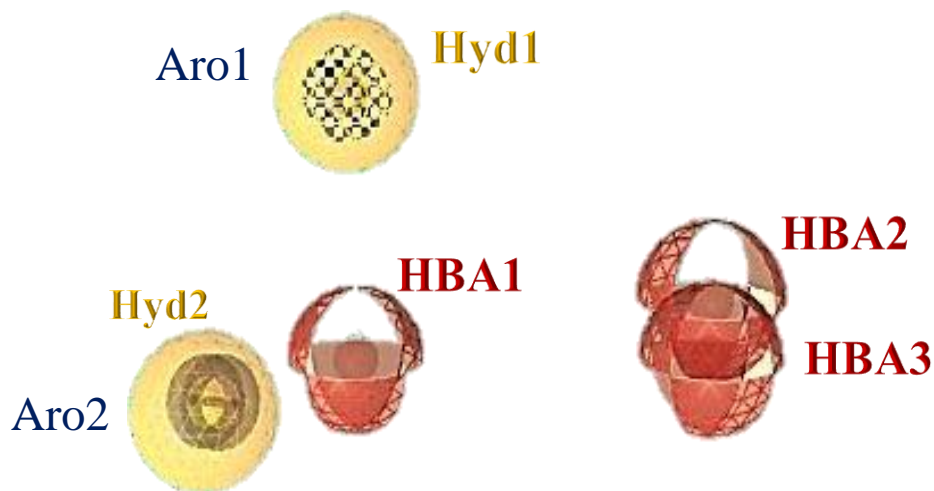


Figure 2.2: The figure shows the features on which the pharmacophore model was built.

Table 3.1: This Table shows the distances measured between features.

	Hyd ₁	Hyd ₂	Aro ₁	Aro ₂	HBA ₁	HBA ₂	HBA ₃
Hyd ₁	0	6.65	0.03	6.43	5.48	8.45	9.17
Hyd ₂	0.65	0	6.63	0.26	3.92	10.47	10.54
Aro ₁	0.03	6.63	0	6.41	5.47	8.43	9.15
Aro ₂	0.48	0.26	6.41	0	3.7	10.29	10.36
HBA ₁	5.48	3.92	5.47	3.7	0	7.96	7.73
HBA ₂	8.45	10.47	8.43	10.29	7.96	0	1.65
HBA ₃	9.17	10.54	9.15	10.36	7.73	1.65	0

- **Screening**

After building the model, it was tested against a dataset of 34 compounds known to be inhibitors. This was done by creating a screening database with a .ldb extension. The screening process identified 14 compounds as hits, resulting in a hit rate of 42.42%. From this, the true positive (TP), true negative (TN), false positive (FP), and false negative (FN) rates were determined. The hit rate is given as and with the total number of the compounds, 14 (42.42%), the conditions are that 16 are active and 18 are inactive listed in the table shown below.

Table 1.2: Table shows statistical parameters and distance matrix for the

Metric	Formula	Calculation
Total Compounds	-	34
Active Compounds	-	16
Inactive Compounds	-	18
True Positives (TP)	-	9
True Negatives (TN)	-	13
False Positives (FP)	-	5
False Negatives (FN)	-	7
Accuracy	Accuracy = (TP + TN) / Total Compounds	Accuracy = (9 + 13) / 35 = 64%
Sensitivity	Sensitivity = TP / (TP + FN)	Sensitivity = 9 / (9 + 7) = 56%
Specificity	Specificity = TN / (TN + FP)	Specificity = 13 / (13 + 5) = 72%

- **Screening of Natural Compounds against Pharmacophore model**

In this study, a comprehensive analysis was conducted using data extracted from the ZINC database, initially consisting of 2,924 natural compounds. To identify potential inhibitors, five Cytochrome P450 (CYP) models were applied to this dataset. This step was crucial in differentiating inhibitors from non-inhibitors. As a result of this screening, the dataset was refined to 1,556 non-inhibitor compounds. These non-inhibitors were then subjected to generate confirmations using MOE software to validate their classification.

Following the validation, the confirmed 1,556 non-inhibitors underwent a secondary screening process using the hERG model to identify any potential hERG inhibitors. This step yielded 177 hits that were identified as hERG inhibitors. After excluding these inhibitors, the remaining 1,379 non-inhibitor compounds were further analyzed by screening them against a pharmacophore model. This sequential and methodical screening process effectively refined the dataset, isolating specific compounds as potential hits for further investigation. This approach not only narrowed down the pool of candidate compounds but also provided a focused pathway for the discovery of effective and safe natural inhibitors.

- **Molecular Docking Against Potential Hits**

After the potential hits were identified using the pharmacophore model, molecular docking was conducted using the GOLD software to assess their interactions with TAS2R4 and TAS2R14 proteins. These proteins were selected due to their significant roles as bitter taste receptors, which are known to influence not only taste perception but also play a part in various physiological processes such as metabolic regulation and gastrointestinal function. The docking with TAS2R4 and TAS2R14 aimed to reveal the molecular interactions and binding affinities of the compounds, providing insights into their potential as modulators or inhibitors. GOLD software was chosen for its advanced algorithms that enable accurate simulation of flexible ligand docking, making it highly suitable for detailed binding studies. This method allowed for a thorough investigation of how these compounds fit into the receptor sites, assessing their potential effectiveness and specificity. The results from this docking study are crucial for further refining the selection of compounds, guiding subsequent experimental validations, and aiding in the development of new agents that could modulate or inhibit these key taste receptors, with possible therapeutic applications.

3.10.2 Molecular Docking for TAS2R4 Blockers

Molecular docking was done through GOLD Suite software. Before starting the docking preparation of ligands is mandatory.

- **Ligand preparation of Inhibitors of TAS2R4**

Table 3.4: Inhibitors of Bitter taste receptor TAS2R4

SER NO	Inhibitors of TAS2R4	PubChem ID	IC ₅₀ Value	References
1	Abscisic Acid (ABA)	643732	34400	[40]
2	N α , N α -bis (carboxymethyl)-l-lysine (BCML)	15691194	59	[53]
3	γ -aminobutyric acid (GABA)	119	3200	[53]
4	GIV3727 or 4- (2,2,3- trimethylcyclopropyl) butanoic acid	25099817	108000	[41]

Structures of potential competitive inhibitors for hTAS2R4 listed in **Table 3.2** were retrieved from the PubChem database in SDF format.

- **Protein Preparation**

Preparation of TAS2R4 structure is already done in the **section 3.9** as shown above.

- **Docking Procedure for Competitive Inhibitors of TAS2R4**

Molecular docking was performed to identify the most probable binding conformations of modulators of selected biological targets using GOLD suite v.5.3.0.[54]. The homology model of TAS2R4 were used in the molecular docking studies. GOLD software, which is known for its accuracy and reliability in ligand-protein interaction prediction, was utilized.

- **Binding Site Prediction for TAS2R4**

For TAS2R4, a comparative method was used to determine the binding position. Because of the two proteins' perfect superimposition and high degree of structural similarity, the structure of TAS2R4 was predicted using the 7PX4 entity 5 template. The structural alignment validated

7PX4's applicability as a template for the homology model TAS2R4. After then, the essential residues found in 7PX4's entity 5 binding site were precisely determined. [51]

The MOE (Molecular Operating Environment) Site Finder tool was used in order to further optimize the binding site residue selection for TAS2R4. This method identified possible binding pockets and crucial residues involved in ligand binding by analyzing the homology model of TAS2R4. The residues were cross-checked detected in the 7PX4 entity 5 binding site with those discovered by the MOE Site Finder which are Leu159, Val160, Thr162, Arg163, Asn164, Phe168, Glu172, and Ser277. The residues chosen for the docking studies were the most precise ones, due to the dual-validation technique. However, binding site of proteins was selected around the 18A region that includes all the active residues identified from literature and the coordinates was selected as X: 1.6769, Y: -0.8237, Z: 13.2187.

- **Poses Generation**

Both the ligand and protein were considered flexible by performing a total of 100 genetic algorithm runs per molecule using the gold score fitness function to enhance the conformational space. 10 poses were generated per compound. The best pose with the highest Dock score was selected for each molecule to explore the protein-ligand interactions inside the binding cavity of TAS2R4.

- **Correlation Analysis**

To predict the binding hypothesis and to reduce the conformational space, a strategies have been applied such correlation analysis between, PIC₅₀ and docking score. For TAS2R4, the final pose for simulations was selected based on high correlation between PIC₅₀ and docking score.

3.11 Molecular Dynamic Simulations (MD)

The docked complexes of TAS2R4 Blockers were followed by MD simulation using Desmond package of Schrodinger software [55]. Three complexes for TAS2R4 were finalized for MD based on their pose analysis study. For MD initially the complexes Structures were energy minimized using force filed of MMFF94S then preprocess at a pH of 7.4. Moreover, the optimized potentials OPLS3e force field were used for the complex simulation.

Furthermore, convergence of Heavy Atom (HA) count was set to RMSD of 0.3 in this system to determine the protein TAS2R4 interactions with efficient ligand molecules. The complex was solvated with the simple point charged (TIP3P) water model. The cubic water box was used to create a 10 Å buffer region between the protein atoms and box sides. The ions were recalculated and neutralized with Na⁺ ions and Cl⁻ ions around the region of 5 Å at a

concentration of 0.15. The OPLS3e force field was used for energy calculation and the temperature was maintained at 303 K. MD simulations for TAS2R4 were executed at 100 ns respectively. The behavior and interactions between the ligands and protein were analyzed using the Simulation Interaction Diagram tool implemented in Desmond MD package.

The stability of MD simulations was monitored by the RMSD of the ligand and protein atom positions in time. Moreover, hydrogen bond histogram has also been analyzed to identify a large fraction of the least stable H-bonds in a conformation.

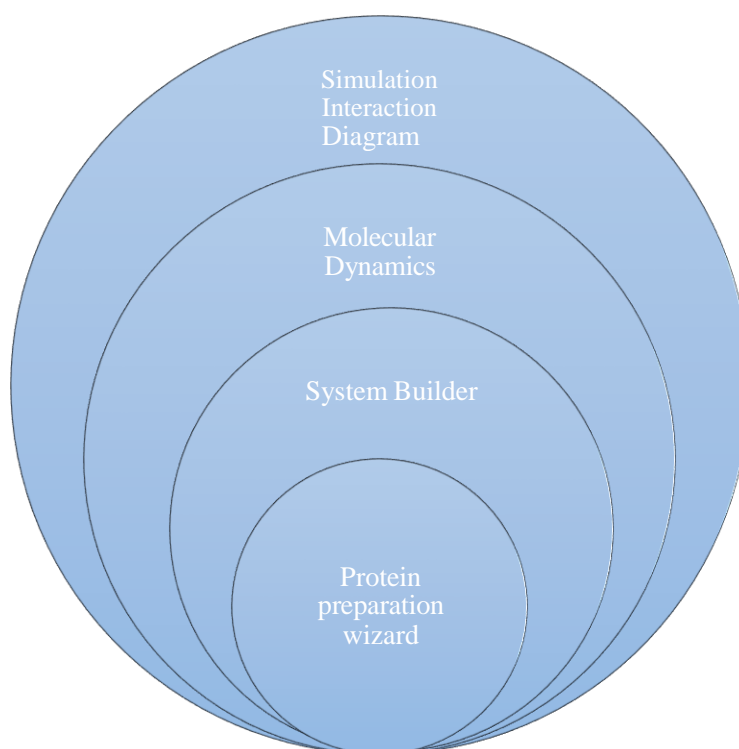


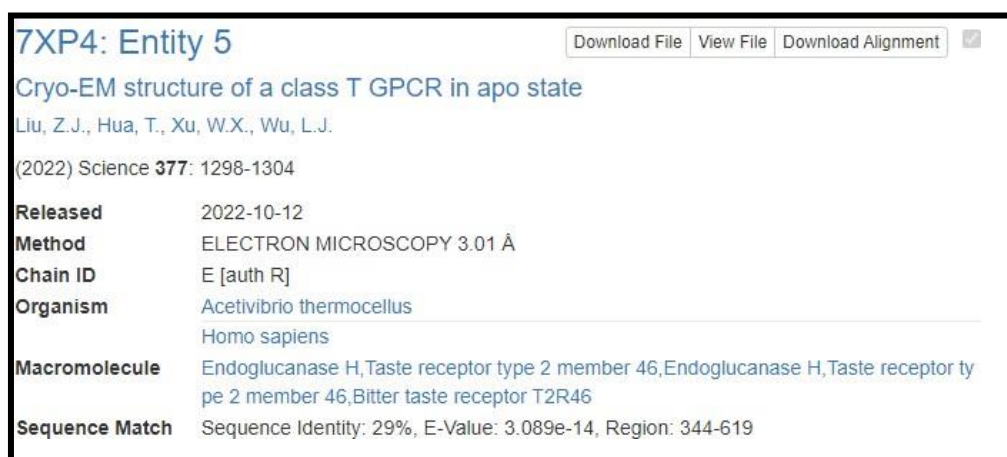
Figure 3.3: Workflow for Molecular Dynamic Simulation.

The overall workflow for molecular dynamics (MD) simulations begins with the protein preparation wizard, which creates the protein structure by adding missing atoms and optimizing the geometry. Next, System Builder sets up the simulation environment, including solution and ion placement. Molecular dynamics simulations are then performed to study the dynamic behavior of the protein-ligand complex over time. Finally, the simulation interaction diagram analyzes and visualizes the interactions and stability of the complex throughout the duration of the simulation.

Chapter 4: Results and Discussion

4.1 Homology Modelling TAS2R4

As the TAS2R4 crystal structure is not available the Sequence was retrieved from uniprot (The UniProt Consortium, 2015). Using the crystal structure of the GPCR protein (PDB code: 7XP4, Entity 5, Chain E) as a template selected due to its 29% sequence similarity to TAS2R4—the homology modeling of TAS2R4 was carried out using the Modeller service. The TAS2R4 amino acid sequence (accession no. Q9NYW5) was obtained from UniProt as the first step. After being formatted into the PIR, the target sequence was repeatedly aligned using relevant templates. Python scripts were run using Modeller to align the TAS2R4 sequence with the recognized templates. A new model was then constructed using the alignment data. The server's ability to sequence alignments made sure that precise and thorough 3D models were built throughout the process.



7XP4: Entity 5 Download File View File Download Alignment

Cryo-EM structure of a class T GPCR in apo state
Liu, Z.J., Hua, T., Xu, W.X., Wu, L.J.
(2022) *Science* **377**: 1298-1304

Released	2022-10-12
Method	ELECTRON MICROSCOPY 3.01 Å
Chain ID	E [auth R]
Organism	Acetivibrio thermocellus Homo sapiens
Macromolecule	Endoglucanase H, Taste receptor type 2 member 46, Endoglucanase H, Taste receptor type 2 member 46, Bitter taste receptor T2R46
Sequence Match	Sequence Identity: 29%, E-Value: 3.089e-14, Region: 344-619

Figure 4.1: Figure shows the template (7XP4) taken for TAS2R4.

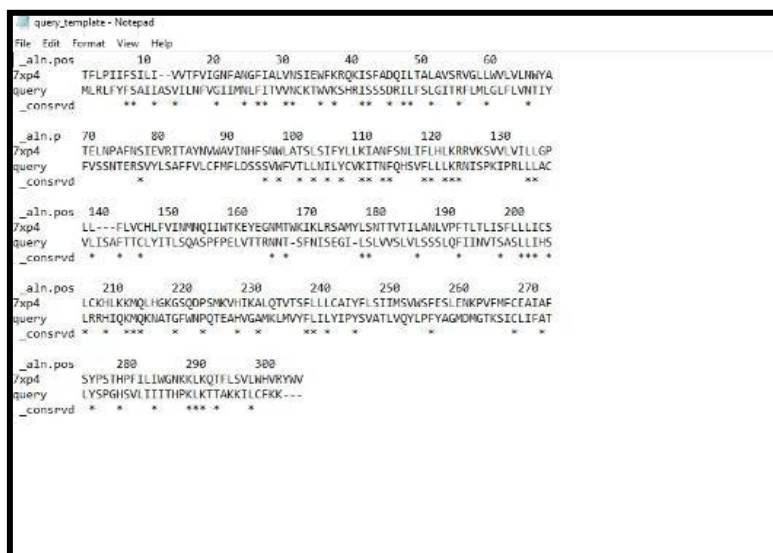


Figure 4.2: Sequence alignment of (TAS2R4) and (7XP4) Contains.

Figure 4.2 explains that the trans membrane portions and important functional motifs of TAS2R4 and 7PX4 show useful conservation in the alignment, while gaps indicate areas where the sequences diverge. The protein's ability to function while maintaining its structural integrity depends on the conserved residues.

Five distinct models of TAS2R4 were generated from modeller, each evaluated based on their scoring metrics, including geometric and energetic properties. It was observed that the first model achieved the highest score among all. Therefore, the first model was selected for further analysis and application due to its highest score.

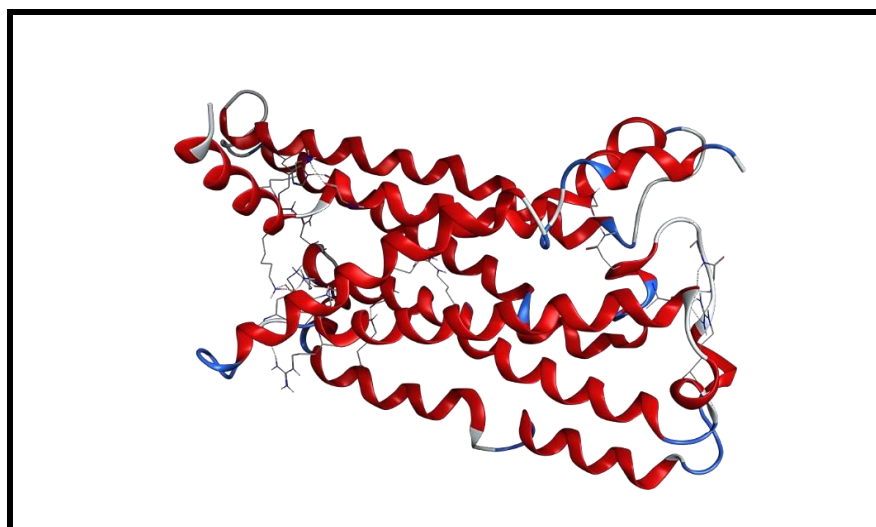


Figure 4.3: Best predicted structure model of TAS2R4 based on their highest score.

4.2 Loop Modelling of TAS2R14

Preparation and refinement of the TAS2R14 structure was successfully achieved through a complex process involving removal of bound molecules and modeling of missing loop regions. Initially, cryoEM structures of Gi-coupled TAS2R14 (PDB identifier: 8VY7) with bound cholesterol, intracellular tastant, and ligand were isolated using Chimera software, focusing on the apo form of the protein. The resulting structure, consisting of 637 amino acids and a particularly chain E, was stored in PDB format for later analysis. The integrity and functional relevance of the TAS2R14 protein was maintained throughout this process, ensuring that the results are applicable to human biology and taste perception.

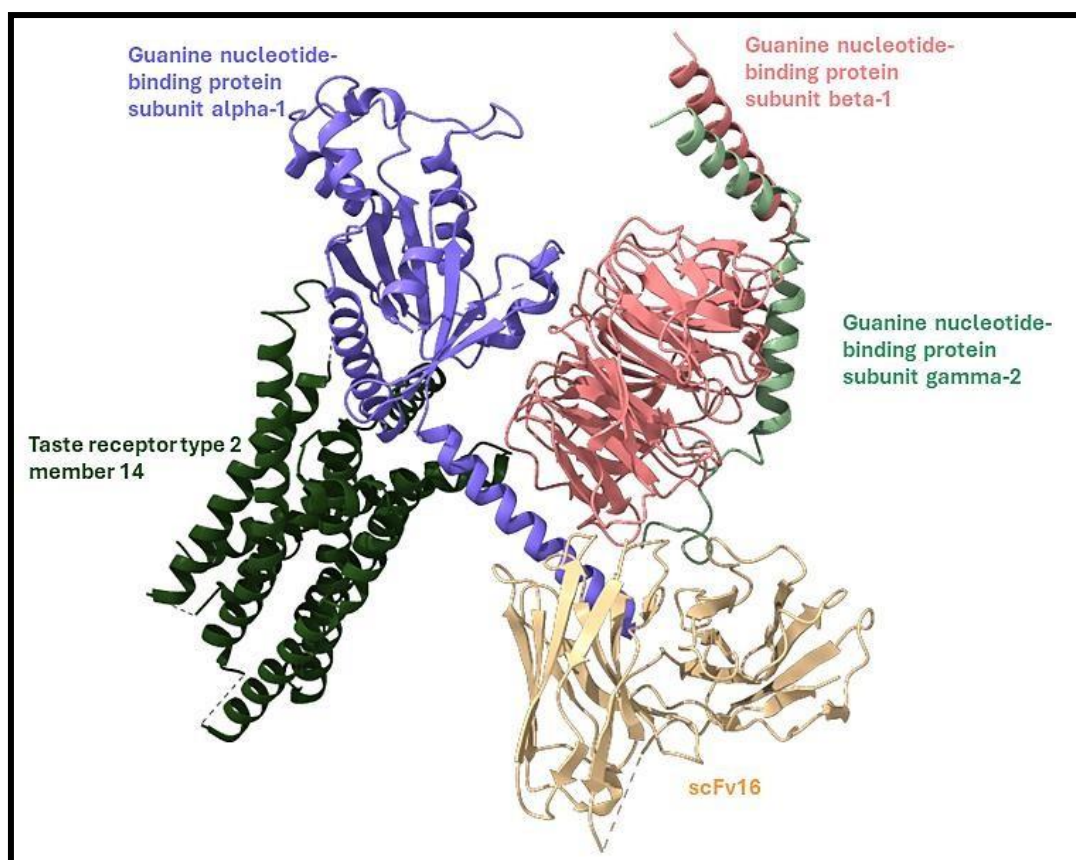


Figure 4.4: Shows the 8VY7 CryoEM structure of Gi-coupled TAS2R14 with cholesterol and an intracellular tastant.

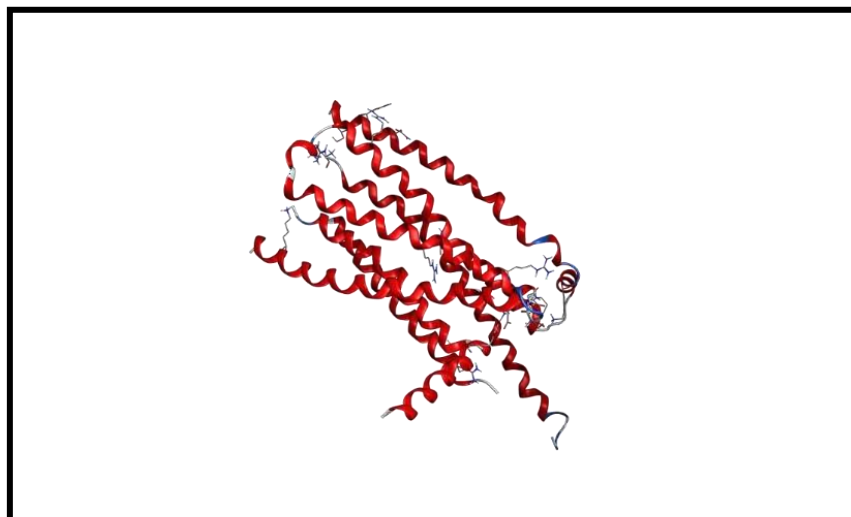


Figure 4.5: It shows the TAS2R14 structure.

Loop modeling resolved the missing residues in the TAS2R14 structure, specifically targeting 159–173, 220–224, and 254–258. Using ChimeraX, advanced algorithms predicted and generated five separate models for these regions. The Z-DOPE score was used to evaluate these models, with the highest scoring model (-0.3) selected for further refinement. This refinement process involved integrating selected loop models into the full TAS2R14 structure, ensuring a realistic and clearly favorable conformation. The final optimized structure was stored in PDB format, providing a comprehensive model of TAS2R14 ready for further computational analyses, such as dynamic simulations and molecular docking, which will help elucidate the protein's role in taste perception. and possible interactions with other flavors.

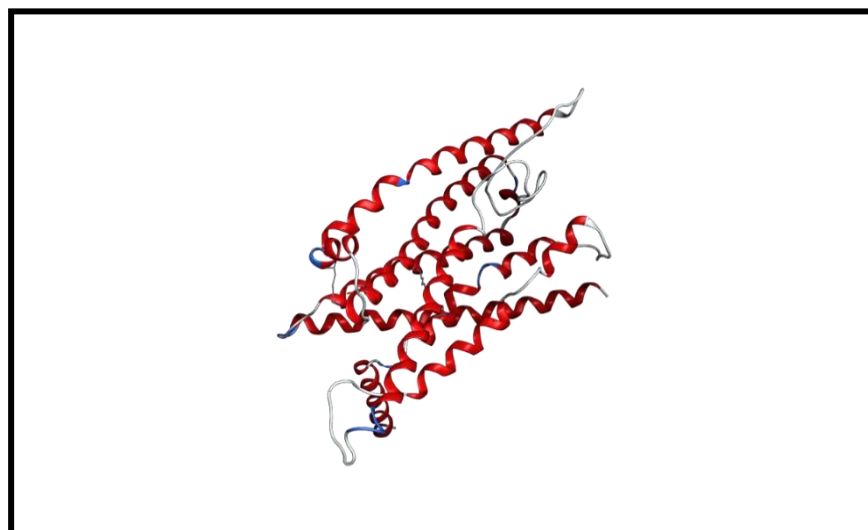


Figure 4.6: It shows the Loop model of TAS2R14 after loop modeling.

4.3 Molecular Dynamic Simulation Analysis of TAS2R4

The MD simulations were done to understand the dynamic behavior of TAS2R4 under physiological conditions and their interaction with the agonist. First, the TAS2R4 structure was minimized in energy using the Amber 99 force field in MOE software, which did minimize steric clashes effectively. Thus, the MD simulations were further post-processed at a physiological pH of 7.4 using the Schrödinger suite to ensure a proper protein structure for physiological conditions. These structures were further used for MD simulations in the OPLS3e force field, which describes molecular interactions reasonably.

The TAS2R4 protein was solvated in the SPC water model within an orthorhombic water box, keeping a buffer zone of 10 Å around the protein atoms. This would maintain a balance in the ionic atmosphere by adding Na⁺ and Cl⁻ ions, which are to be used in neutralizing the system. Temperatures were kept fixed at 303 K during the MD simulations conducted for 100 nanoseconds to conduct detailed analyses of the dynamic behavior of TAS2R4. In this respect, Desmond MD package simulation interaction diagrams were used for a further, detailed look into protein-ligand interactions and conformational changes through simulation.

The stability and accuracy of the MD simulations were checked through the root mean square deviation and root mean square fluctuation of protein atoms. The RMSD values were within the 0.3 Å equilibrium tolerance, proving sufficiency for the equilibration of the system. In addition to that, the RMSF analysis gave information about flexibility or several protein regions showing places with conformational stability or dynamical motion. In all, MD simulations provided an overview of the conformational dynamics and functional properties for TAS2R4, thereby furnishing significant insights into its mechanistic role in taste perception and its potential interactions with ligands.

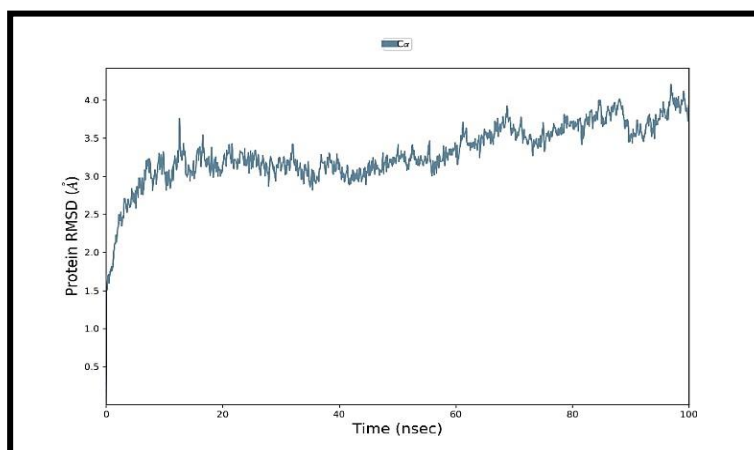


Figure 4.7: RMSD profile of TAS2R4 protein during MD simulations at 100ns.

Figure 4.7 shows the graph illustrates the RMSD of the TAS2R4 protein during a 100 nanosecond molecular dynamics (MD) simulation. Initially, the RMSD increases significantly, reflecting rapid changes as the protein adapts to the simulation environment. After this spike, the RMSD stabilizes but continues to fluctuate, indicating ongoing dynamic adjustments in the protein structure. Overall, the RMSD trended upward throughout the simulation, suggesting that the protein explores different conformational states, possibly settling into a new structure by the end of the simulation period. This analysis is important for insight into protein behavior, which is important for applications such as drug design and protein engineering.

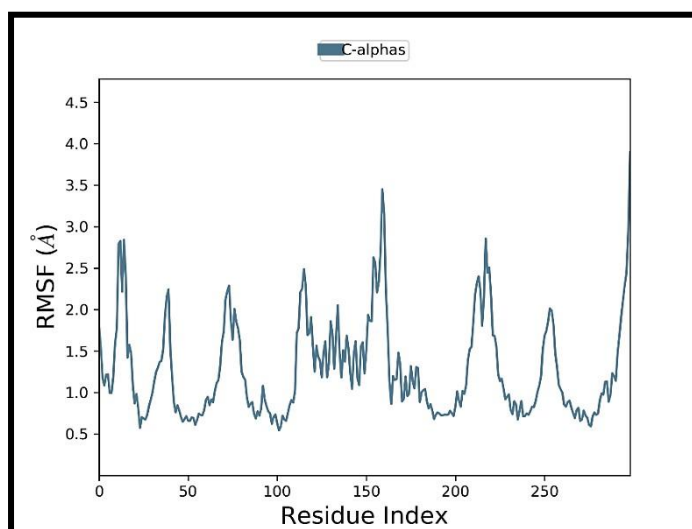


Figure 4.8: Root Mean Square Fluctuation (RMSF) plot for TAS2R4.

Figure 4.8 explains the dynamics behavior of every residue during molecular dynamics simulation. The peaks in the plot of RMSF refer to the regions with a high degree of flexibility or motion within the protein structure. Notice how there are substantial peaks appearing at distinct residual indices, which are pointing out locations of high flexibility. The peaks correspond to fluctuations of residues TYR_159, LYS_163, SER_166, ASP_168, ARG_174, ALA_222, LYS_225, ARG_256, and GLU_258. These residues demonstrate high RMSF values and, therefore, must belong to flexible loops or regions within the protein. The data outline the regions in the TAS2R4 protein that are dynamically active and hence could be important for its functional interactions and stability.

4.5 Molecular Dynamic Simulations of Loop Model TAS2R14

MD simulations of the loop model of the TAS2R14 protein structure gave a detailed understanding of the dynamic behavior of this structure under physiological conditions. First

of all, the TAS2R14 structure was energy-minimized with the force field Amber99 within the MOE software; this removed steric conflicts and other non-favorable interactions. The reduced structures were then pre-processed at a physiological pH of 7.4 and loaded into the Schrödinger suite for running the MD simulation. Using the OPLS3e force field, the simulations reproduce very well molecular interactions, with already converged heavy atom counts to within an RMSD of 0.3 Å that will ensure proper equilibration.

The structure of TAS2R14 was solved using the TIP3P water model in a cubic water box; this preserved a 10 Å buffer zone around protein atoms. To neutralize the system, Na⁺ and Cl⁻ ions were added and then recalculated to achieve a concentration of 0.15 M within the 5 Å zone. MD simulations were run at a constant temperature of 303 K for 100 nanoseconds to permit a longer assessment of the protein dynamics. Simulation interaction diagrams within the Desmond MD package were applied to detail protein-ligand interactions and conformational changes.

The stability and accuracy of the MD simulations were checked by looking at the root mean square deviation of protein atom positions with respect to time. The RMSD analysis showed stable convergence; therefore, it had equilibrated and gave reliable insight into the dynamic properties of TAS2R14. These MD simulations of loop model of TAS2R14 gave a good view of TAS2R14's conformational dynamics and interactions, which contribute to knowledge about its functional properties during taste perception and possible interactions with other molecules.

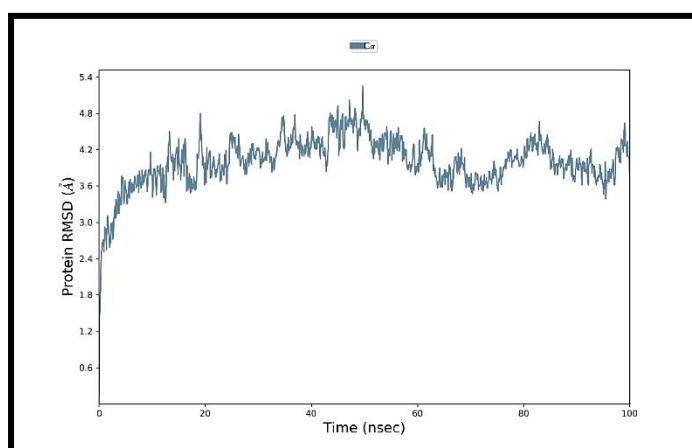


Figure 4.9: RMSD profile of TAS2R14 protein during MD simulations at 100ns.

Figure 4.9 shows the graph shows the root mean square deviation (RMSD) of the TAS2R14 protein over a 100 nanosecond molecular dynamics (MD) simulation. The RMSD values, plotted on the y-axis, range from about 1.2 to 4.8 Angstroms and exhibit significant fluctuations

throughout the duration of the simulation, as shown on the x-axis from 0 to 100 nanoseconds. The RMSD fluctuates frequently but generally maintains a level between 3.0 and 4.0 Angstroms, suggesting that the protein experiences ongoing changes while potentially stabilizing within a specific conformational range. This behavior indicates the dynamic nature of the protein under synthetic conditions, highlighting important aspects of its stability and conformational variation.

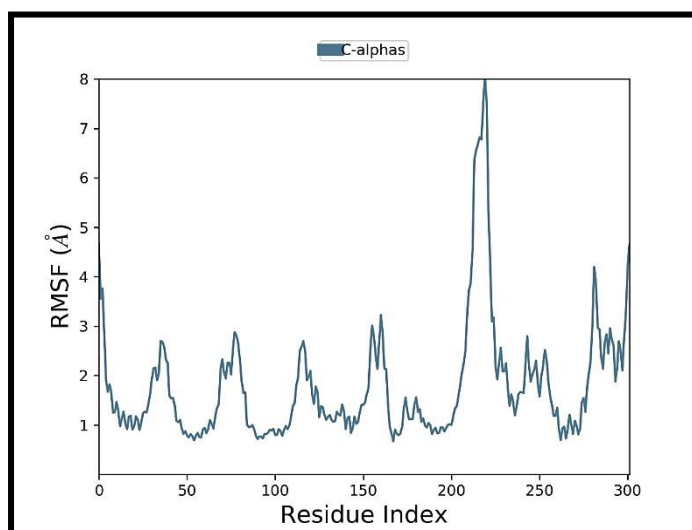


Figure 4.10: Root Mean Square Fluctuation (RMSF) plot for TAS2R14.

Figure 4.10 shows the dynamic behavior of each residue during molecular dynamics simulations. Peaks in the RMSF plot indicate regions of high flexibility or motion within the protein structure. Significant peaks are observed at residues 159–163, 219–225, and 253–259, indicating that these regions show significant flexibility. Residues at these peaks include TYR_159, ARG_160, ASN_162, LYS_163, GLY_220, ASP_221, ALA_222, THR_224, SER_254, GLU_255, ARG_256, and LE75. These residues are likely to be among the regions of the protein that undergo substantial changes. The data highlight regions of the TAS2R14 protein that are dynamically active, which may be important for its functional interactions and stability.

4.6 Molecular Docking TAS2R4 and TAS2R14 Results

Preparation of TAS2R14 and TAS2R4 proteins for docking and subsequent molecular docking studies yielded important insights into the binding interactions of these taste receptors. Initially, the First and Last frame was extracted from MD simulations of both TAS2R14 and TAS2R4 saved in CMS format using Schrödinger software. The structures were then prepared for docking using a molecular operating environment (MOE), where all heteroatoms and water

molecules were removed to prevent non-specific interactions and then last frame was finalized for docking.

Molecular docking was performed using Gold Suite v.5.3.0 to determine the most likely binding conformation of the modulators for TAS2R14 and TAS2R4. For TAS2R14, binding site prediction was based on the literature, identifying key residues such as Ile62, Phe76, Phe82, Leu85, Trp89, Ile179, Val180, Thr184, Ile187, Phe188, Phe243, Phe247, Ile262. The docking site was centered in a 20Å region around coordinates X: -2.7387, Y:-1.6913, Z:-4.993. For TAS2R4, a comparative method using the 7XP4 entity 5 template because they were perfectly superimposed as shown in the figure 4.11 so the residues which were found in the 7XP4 literature were selected for the TAS2R4 and also crossed check through the MOE Site Finder tool which identified the key residues such as Leu159, Val160, Thr162, Arg163, Asn164, Phe168, Glu172, and Ser2773. The docking site for TAS2R4 was centered in an 18Å region around the coordinates X: 1.8296, Y: -0.1408, Z: 12.561. Flexible docking was performed with 100 genetic algorithm runs per molecule, generating 10 poses per compound. The best pose with the highest docking score was selected to explore protein-ligand interactions.

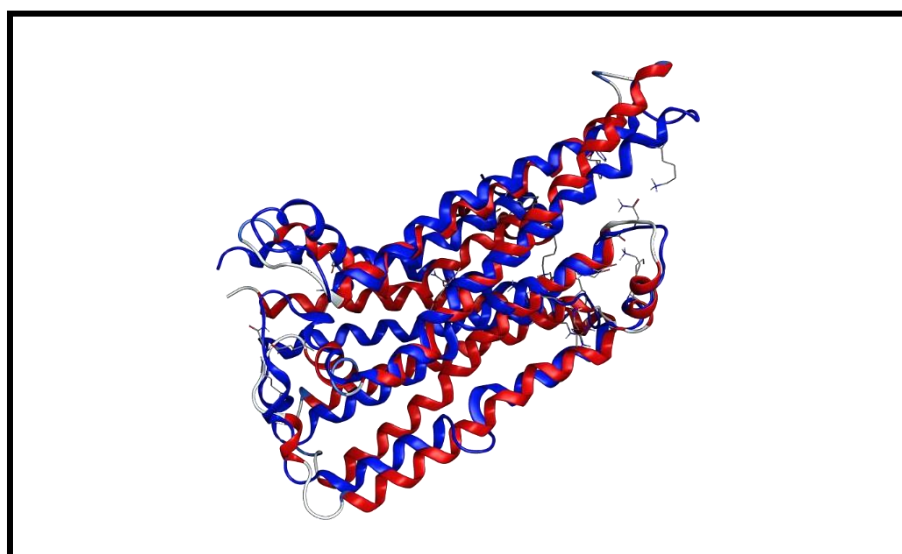


Figure 4.11: The red color shows TAS2R4 structure and blue color shows 7XP4 structure are perfectly superimposed.

Ramachandran plots generated using the Swiss model confirmed the structural integrity of the protein, indicating minimal residues in disallowed regions, thus ensuring the stability of the protein structure. The processed protein structures were saved in PDB format, ready for docking studies.

- **TAS2R4**

The Ramachandran plot for the first frame as shown in figure below 4.12 (A) extracted from the MD simulation of TAS2R4 provides an insight into the dihedral angles ϕ (phi) and ψ (psi) of the amino acid residues. The plot shows that a significant fraction of residues (85.19%) are located in highly favored regions, indicated by densely populated green regions, corresponding to stable α -helical and right-handed α -helical conformations. . Additionally, light green regions represent permissive regions that accommodate β -sheet structures and left-handed α -helices, indicating the structural flexibility of the protein. In particular, a small percentage (2.36%) of residues, such as A174, V14, A12, E172, A11, and L255, are found in dissociated regions. These outliers likely reside in loops, bends, or flexible regions that do not conform to regular secondary structure. An overall MolProbity score of 2.27 and a collision score of 2.65 further illustrate the favorable conformation of the protein, with most residues adopting energetically stable positions. This comprehensive analysis highlights the structural integrity and flexibility of the TAS2R4 protein as captured in the first frame of the MD simulation.

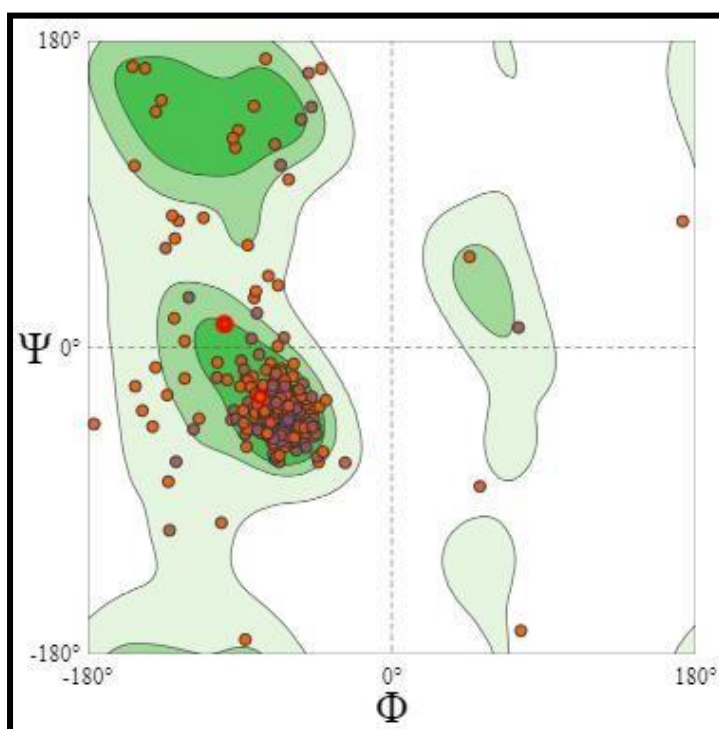


Figure 4.12: A) Ramachandran plot for the first frame of TAS2R4 Structure.

The Ramachandran plot for the final frame as shown in figure below 4.12 B) derived from MD simulations of TAS2R4 indicates a highly favorable protein conformation, with 90.91% of residues located in the most favored regions, namely stable α -helical and right-handed α -helical structures. Are equivalent to light green allowed regions accommodate additional residues,

increasing the structural flexibility of the protein. Only 0.34% of residues, such as A168 PHE, are found in disapproved regions, reflecting the minimal presence of outliers. A MolProbity score of 1.91 and a collision score of 2.24 further confirm the high quality and stability of the protein structure.

This plot indicates the essentially stable and well-folded nature of the TAS2R4 protein, with a very low percentage of residues in conformational conformations.

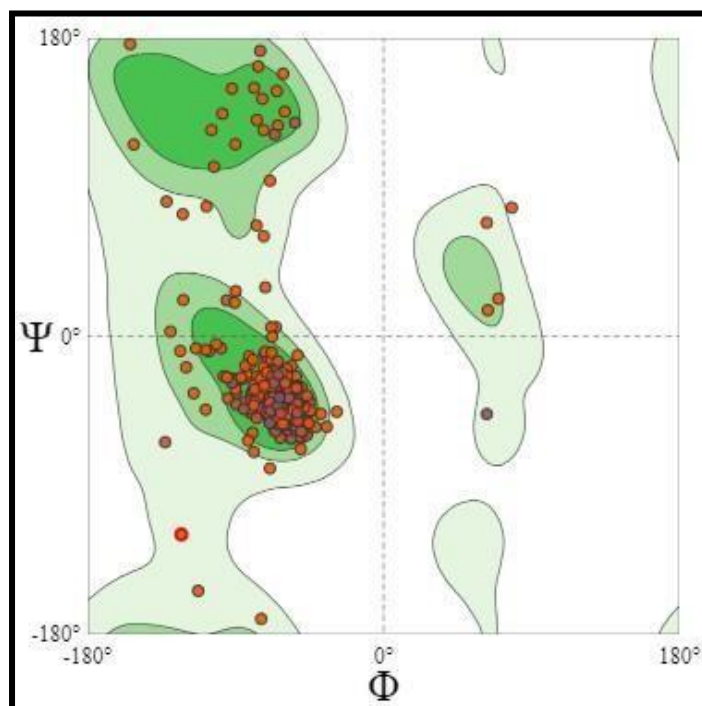


Figure 4.12: B) Ramachandran plot for the final frame of TAS2R4 Structure.

The Ramachandran plot for the first frame as shown in figure 4.13 (A) extracted from the MD simulation of TAS2R14 indicates a generally favorable protein conformation. The plot shows that 83.87% of the residues are in highly favored regions, indicated by densely populated green regions, suggesting that the protein mainly adopts stable α -helical and right-handed α -helical conformations. Allowed regions, represented by light green regions, accommodate an additional set of residues, increasing the structural flexibility of the protein. However, 5.02% of residues, such as A279 VAL, A218 ILE, and A282 LEU, are found in disallowed regions, highlighted by red circles, indicating less favorable conformations associated with loops, turns, or flexible regions. A MolProbity score of 2.10 and a collision score of 1.41 further reflect the overall quality of the structure.

The presence of rotamer outliers (5.24%) and C-beta deviations suggests that minor conformational adjustments may be necessary, but overall, the protein structure maintains a high degree of stability and proper folding as most Residues are shown to be in favorable areas.

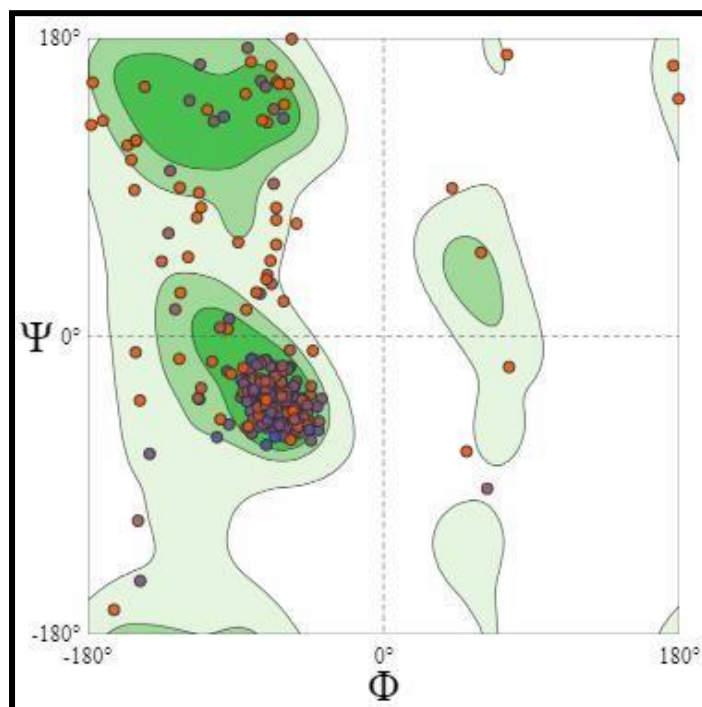


Figure 4.13 A): Ramachandran plot for the first frame of TAS2R14 Structure.

The Ramachandran plot for the last frame as shown in the figure below 4.13 (B) derived from the MD simulation of TAS2R14 shows that 87.10% of the residues are within the highly favored regions, indicated by the densely populated green regions, which are stable α -helical and right-handed α - reflects the helical conformation. The light green allowed regions to accommodate additional residues, contributing to the protein's structural flexibility. 2.51% of residues, such as A33 ILE, A244 SER, A201 LEU, A79 GLU, A175 PHE, A172 PHE, and A183 SER, are found in disallowed regions, which are usually, suggesting less favorable confirmations. Bends, or flexible areas. A MolProbity score of 1.77 and a collision score of 1.81 indicate a high-quality protein structure. Rotamer outliers accounted for 1.87%, while C-beta deviation was observed in 42 cases. Overall, the plot highlights that the TAS2R14 protein maintains an essentially stable and well-folded structure with a minimal percentage of residues in disallowed regions.

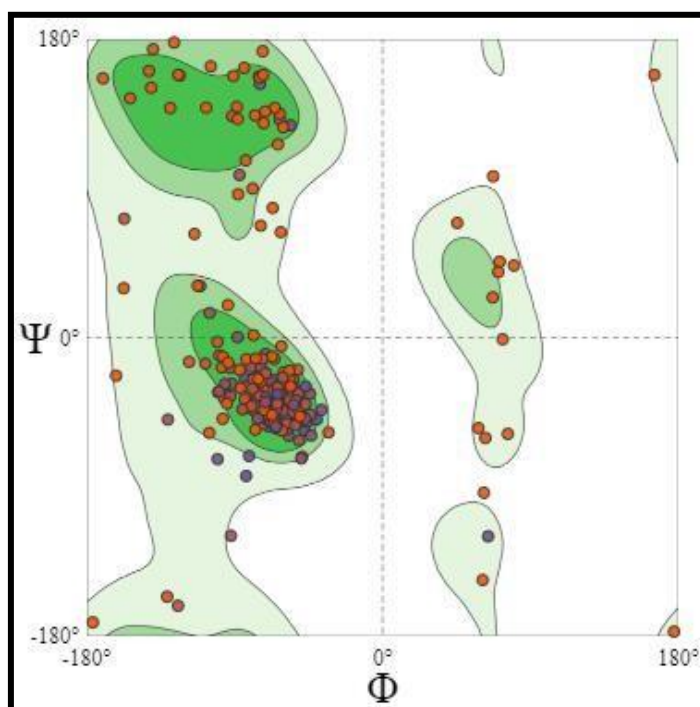


Figure 4.13: B) Ramachandran plot for the last frame of TAS2R14 Structure.

The correlation between PIC₅₀ values and docking scores was analyzed to refine binding hypotheses. This analysis ensured that the final poses selected for the TAS2R4 and TAS2R14 simulations had high correlations between PIC₅₀ and docking scores as shown in the both figures below, increasing the accuracy of interaction predictions. Comparative docking simulations on the same dataset of compounds of both proteins allow direct comparison of binding affinities, interaction patterns, and docking scores. This comparative study highlighted similarities and differences in ligand interactions between TAS2R4 and TAS2R14, providing valuable insight into their interaction mechanisms and potential ligand selectivity.

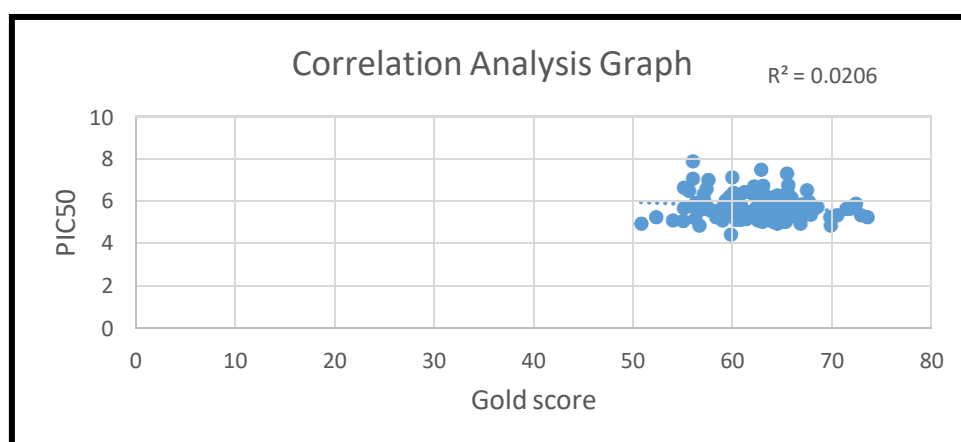


Figure 4.14: A correlation graph for docking score (Gold score) and PIC₅₀ values of TAS2R4.

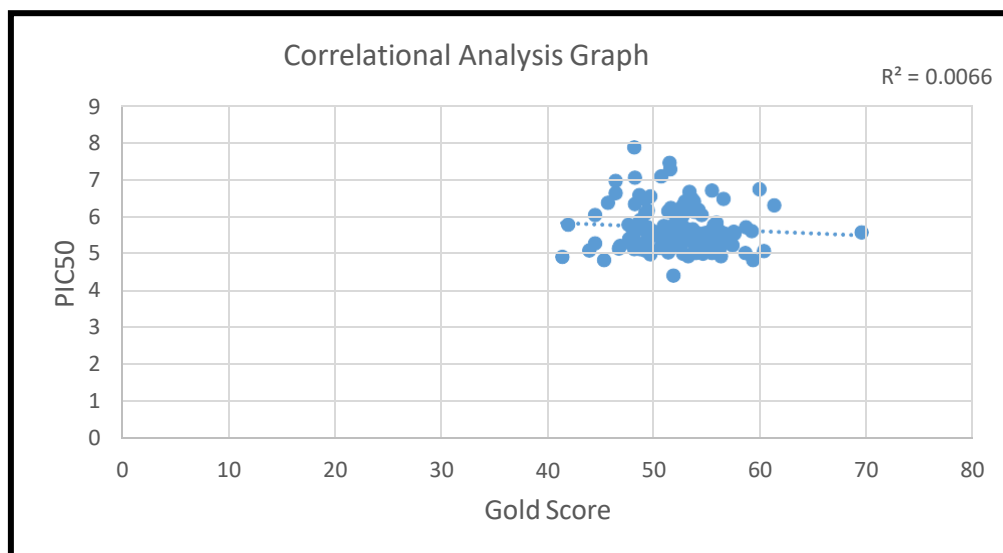


Figure 4.15: A correlation graph for docking score (Gold score) and PIC50 values of TAS2R4.

4.7 Results of Pharmacophore Modeling

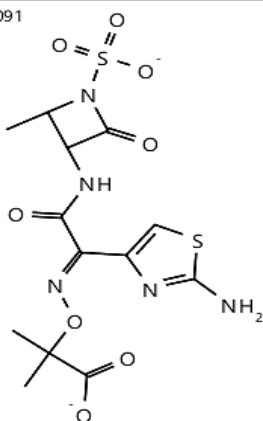
A rigid screening of a carefully constructed pharmacophore model based on a subset of the compounds' docking conformation against a dataset of active and inactive compounds is conducted to evaluate the predictive performance. Finally, a screening library database in the .Ilb format was generated using Ligand Scout software, containing 16 active. The threshold for active compounds was IC₅₀ value less than 400nm above were considered as active, and 18 inactive compounds containing IC₅₀ value greater than 8000nm were considered inactive. It gave an impressive hit rate of 42.42% when this library was screened against the pharmacophore model, which underscores the model's reliability in distinguishing between active and inactive compounds. The model was built using key features such as aromatic, hydrophobic regions, and hydrogen bond acceptors, which are critical in binding interactions. This hit rate reflects the model's strong potential in identifying promising compounds based on these structural features. A pharmacophore model built on the foundation of docking conformations and further validated through a rigorous screening process was found to be highly efficient, achieving an impressive hit rate of 42.42%. This level of accuracy underscores the model's robustness and its potential application in identifying promising compounds for drug development. By forming a solid framework for further experimental validation, this model proves to be an invaluable tool in virtual screening and drug discovery, paving the way for more targeted and efficient drug development efforts.

- **Analysis of Screened Natural Compounds and Molecular Docking**

After screening the natural compounds against the pharmacophore model five potential hits compounds were identified.

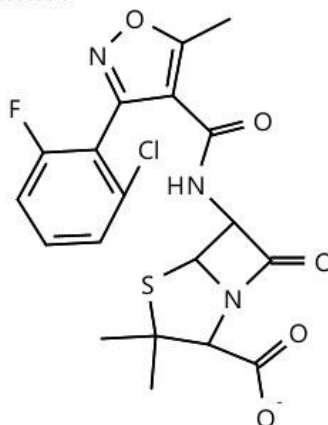
Aztreonam

ZINC12503091



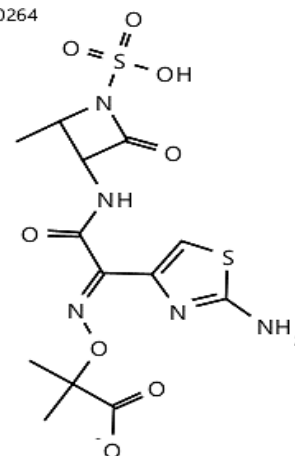
Flucloxacillin sodium

ZINC03830845



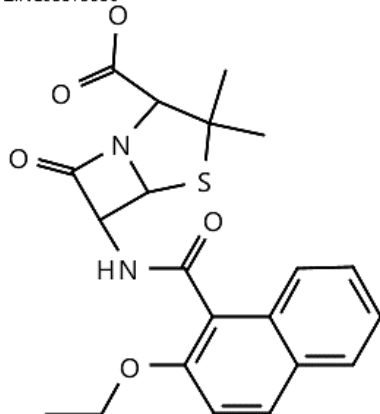
Aminothiazol

ZINC03830264



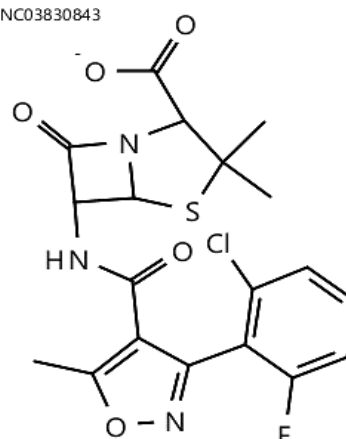
Nafcillin sodium

ZINC03875980 -



Flucloxacillin sodium

ZINC03830843



- **Molecular Docking against Five Potential Hits**

Molecular docking was then conducted for the identified potential hits against TAS2R4 and TAS2R14 proteins using GOLD software. These proteins were chosen due to their significant roles as bitter taste receptors, which are integral to taste perception and various physiological functions such as metabolic regulation and gastrointestinal health. Ligands were prepared using Open Babel software, which involved adding only polar hydrogens and generating both 2D

and 3D coordinates. This preparation was crucial for ensuring accurate docking simulations. The docking results revealed that five compounds demonstrated potential as modulators or inhibitors of these taste receptors. To strengthen the validity of these findings, the docked protein-ligand complexes were visualized, with a detailed examination of the amino acid residues involved in the interactions. These residues were carefully compared to those found in known inhibitors of TAS2R4 and TAS2R14. This comparison was essential for multiple reasons. First, the presence of similar amino acid residues in the binding sites between the natural compounds and known inhibitors suggests that these new compounds could interact with the receptors in a similar fashion. Such structural and functional similarities are often indicative of comparable binding affinities and inhibitory mechanisms, which could imply that these natural compounds may serve as effective modulators by either enhancing or inhibiting the receptor's function. Second, this comparison helps in predicting the potential therapeutic relevance of these compounds. If the new compounds share key binding interactions with known inhibitors, they may be more likely to exhibit desirable pharmacological properties, such as specificity and potency, when targeting these taste receptors. This could lead to the development of new therapeutic agents for conditions related to metabolic regulation, gastrointestinal health, or even taste modulation, where TAS2R4 and TAS2R14 play significant roles. Lastly, understanding the similarities in binding interactions also aids in the rational design of further studies and potential modifications to these compounds. By identifying which amino acid residues are crucial for binding, researchers can hypothesize how altering certain aspects of the compounds might improve their efficacy or reduce unwanted side effects.

4.8 Molecular Docking TAS2R4 Blockers Results

Molecular docking studies for TAS2R4 blockers were conducted using Gold Suite software to determine the most likely binding conformation of competitive inhibitors. Initially, the structures of the potential competitive inhibitors listed in Table 3.2 were retrieved from the PubChem database in SDF format. These ligands were designed for docking, ensuring accurate and reliable interaction predictions. A previously developed homology model of TAS2R4, as described in Section 3.9, was used for these studies. Binding site prediction for TAS2R4 involved a comparative approach using the 7PX4 entity 5 template, which took advantage of the high structural similarity and perfect superimposition between the two proteins. The essential residues identified from the 7PX4 binding site Leu159, Val160, Thr162, Arg163, Asn164, Phe168, Glu172, and Ser277 were further validated using the MOE Site Finder tool.

This double validation technique ensured the selection of exact residues, with the binding site centered on coordinates X: 1.6769, Y: -0.8237, Z: 13.2187 within an 18Å region. Flexible docking was performed with 100 genetic algorithm runs per molecule, generating 10 poses per compound. The best pose with the highest docking score was selected to explore the protein-ligand interactions within the binding cavity of TAS2R4. Such docking simulations have brought to the fore some very important insights into the binding affinities and interaction patterns of TAS2R4 with its inhibitors. The PIC₅₀ values and docking scores were correlated to further bind hypotheses and reduce conformational space. This analysis ensured that the final picked poses for the simulations had high correlation between PIC₅₀ and the docking score as shown in figure 4.16, hence increasing the reliability of the predicted interactions. It gives insight into the detailed mechanism of TAS2R4 interaction with its competitive inhibitors. Results from molecular docking have undoubtedly shed more light on the mechanism of interaction between TAS2R4 and its competitive inhibitors, highlighting the ability of these inhibitors to modulate TAS2R4 receptor function.

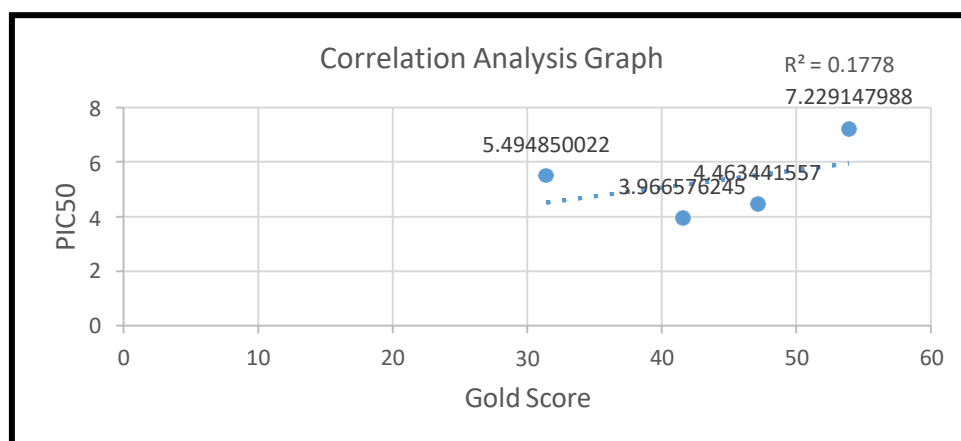


Figure 4.16: A correlation graph for docking score (Gold score) and PIC₅₀ values of TAS2R4 Blockers data.

4.8.1 Molecular Interaction

Correlation analysis graphs for the molecular interactions of TAS2R4 blockers BCML, GABA, and GIV3727 were generated for the final selection of these interactions for MD simulations. The selection of blocker interactions in 2D and 3D formats is shown below.

• Details of the Interaction Between BCML and Protein TAS2R4.

This image is a 3D molecular visualization depicting interactions of BCML (shown in purple) and the TAS2R4 receptor (displayed in cyan) as shown in figure 4.17(B). The residues involved in these interactions are marked and include threonine at position 66 (T66), asparagine at position 169 (N169), isoleucine at position 170 (I170), leucine at position 175 (L175), alanine at position 269 (A269), threonine at position 270 (T270), serine at position 273 (S273), and valine at position 85 (V85). The red dashed lines represent potential hydrogen bonds and hydrophobic interactions, crucial for the stability of the blocker within the binding site of the TAS2R4 receptor, indicating a likely inhibition mechanism of this taste receptor. The 2D interaction diagram as shown in figure 4.17 (A), provides a detailed view of specific interactions between BCML and residues within the TAS2R4 binding pocket. BCML forms important hydrogen bonds with Ile170, Asn65, Asn169, and Glu172, which are essential for ligand stability and binding affinity. Hydrophobic contacts with residues such as Phe88, Leu175, and Ile174 favor a stable fit of the ligand within the binding site.

Furthermore, electrostatic interactions with Glu172 are important for maintaining ligand orientation and binding strength within the pocket. Collectively, these interactions highlight the strong binding affinity and stability of BCML within the TAS2R4 binding site, highlighting its potential as an effective TAS2R4 blocker.

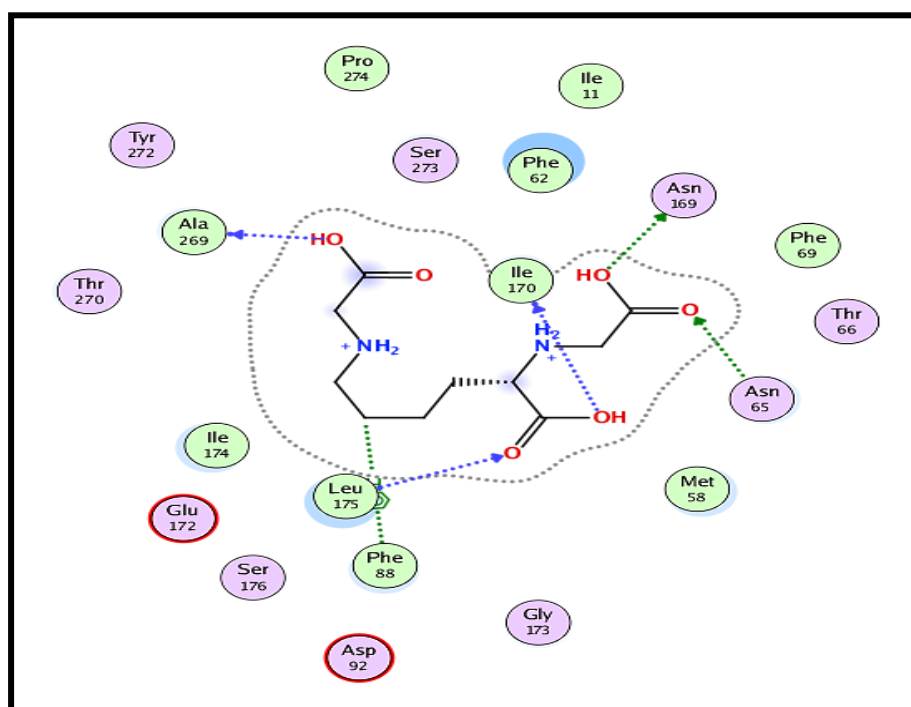


Figure 4.17: A) 2D Interaction Pattern of BCML Ligand and TAS2R4 Protein

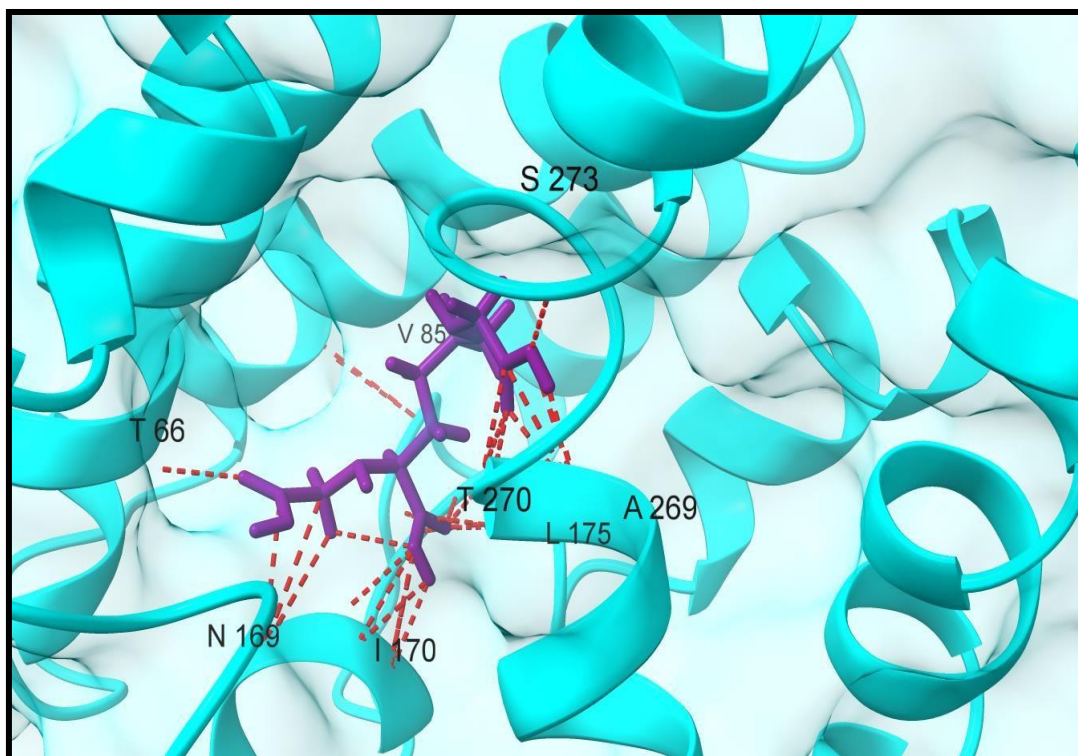


Figure 4.17: B) 3D interactions of ligand BCML with Protein TAS2R14

• Details on the Interaction of GABA with the Protein TAS2R4

In this detailed molecular visualization, the interactions between gamma-aminobutyric acid (GABA) and the TAS2R4 receptor are depicted with enhanced clarity. GABA, shown in purple, is strategically positioned to engage with several key residues of the TAS2R4 receptor, which is rendered in Blue as shown in the figure 4.18. These interactions involve not only the previously noted residues but also additional contacts that likely contribute to the binding affinity and specificity.

The residues such as valine at positions 96 and 99 (V96, V99) and serine at positions 184 and 185 (S184, S185) suggest hydrophobic interactions, while aspartate at position 92 (D92) and arginine at position 55 (R55) could be forming salt bridges or hydrogen bonds with GABA. The placement of tyrosine at position 272 (Y272) indicates possible pi-stacking interactions, which are often critical in stabilizing ligand-receptor complexes.

These molecular interactions are essential for the functional modulation of the TAS2R4 receptor by GABA, potentially altering the perception of bitterness and other taste modalities. Understanding such detailed interactions helps in the design of more effective receptor blockers

or modulators, which could have implications in nutritional science and therapeutics targeting taste receptor pathways.

The 2D interaction diagram indicates, in detail, the interactions of GABA with TAS2R4 as shown in the figure 4.18. GABA forms hydrogen bonds with Arg55 and Asp92, which are important for the stable binding of this ligand. These also show interactions with surrounding residues, including Met58, Ser95, Val99, and Tyr272, that contribute to global stability. Of these interactions, hydrogen bonding and hydrophobic contacts contribute jointly to hold the ligand firmly in the TAS2R4 binding pocket.

The diagrams for 2D and 3D interaction of GABA with TAS2R4 show a clearly defined binding mode that is characterized by strong hydrogen bonds and supportive hydrophobic interactions. These findings identify GABA as a stable and efficient ligand for TAS2R4, with implications for its mechanism of action as a blocker.

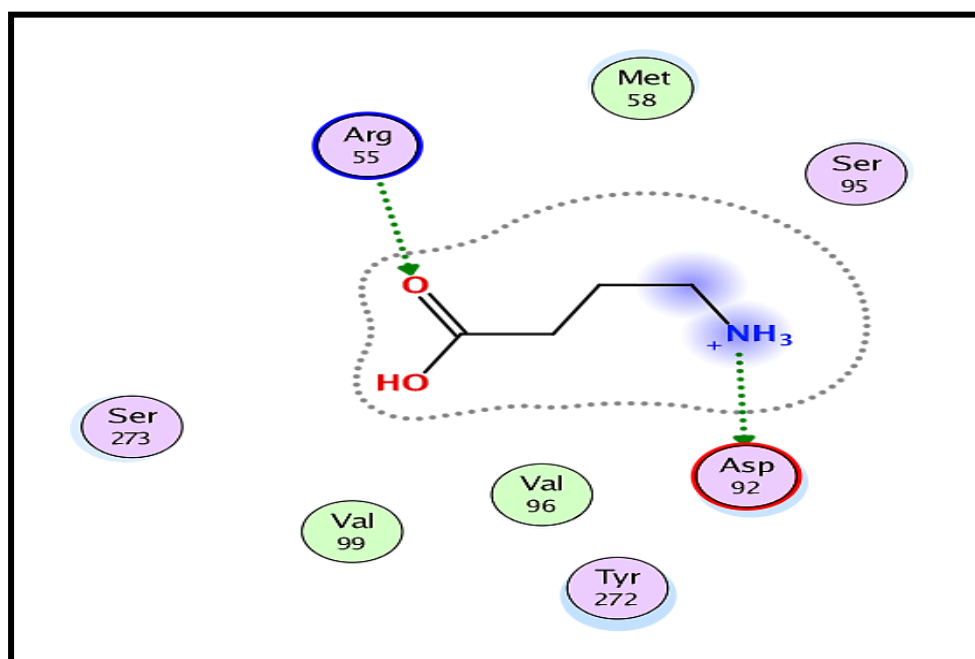


Figure 4.18: A) 2D Interaction pattern of GABA Ligand and TAS2R4 protein.

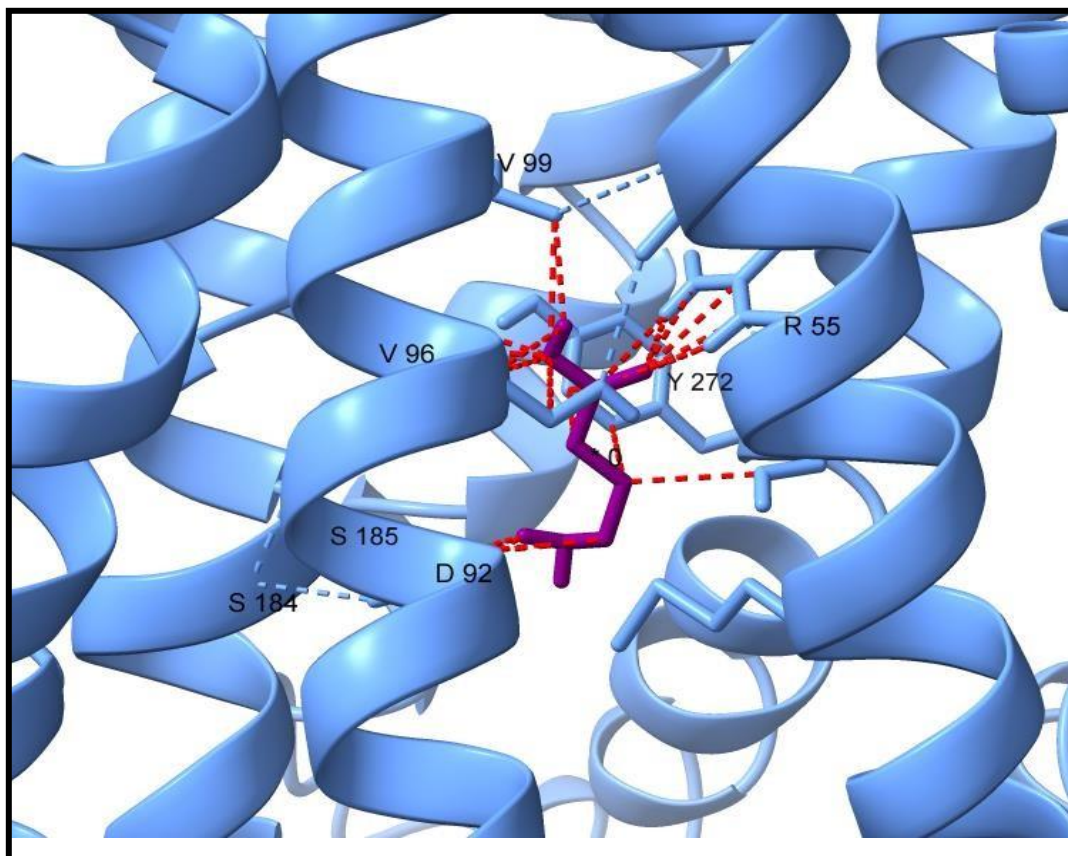


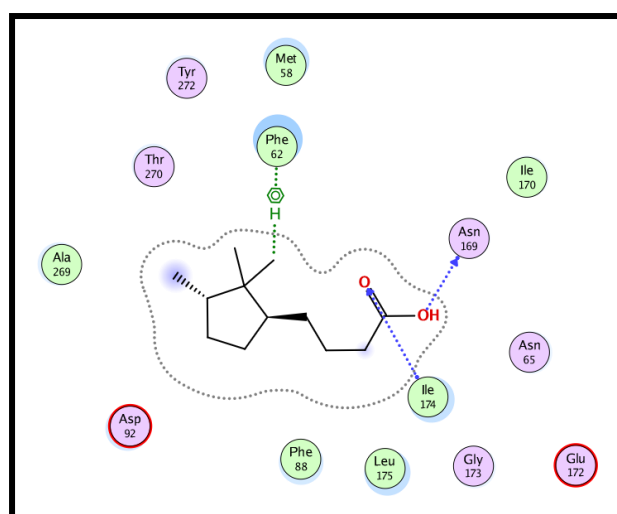
Figure 4.18: B) GABA ligand and protein TAS2R14 3D interactions

- **Details of GIV3727's Interactions with Protein TAS2R4**

This image depicts a 3D molecular visualization of the interactions between the blocker GIV3727 (displayed in red) and the TAS2R4 protein (shown in purple). The visualization highlights several key residues within the TAS2R4 protein that interact with GIV3727 as shown in the diagram below. These residues include asparagine at positions 65 and 169 (ASN65, ASN169), glycine at position 173 (GLY173), threonine at position 170 (THR170), phenylalanine at position 62 (PHE62), isoleucine at position 174 (ILE174), methionine at position 58 (MET58), and alanine at position 269 (ALA269). The interactions, represented by red dashed lines, likely involve a mix of hydrogen bonds and hydrophobic interactions, crucial for the stable binding of GIV3727 to TAS2R4, potentially influencing the receptor's function related to taste perception. This detailed view provides insights into the molecular dynamics and interaction specificity which are essential for the development of targeted therapies or modifiers of taste receptor activity. In the 2D interaction diagram, specific interactions of GIV3727-TAS2R4 are shown in detail. The ligand forms hydrogen bonds with Asn169, Ile174,

and Phe62, which could help in keeping the stable binding conformation. It is also encircled by residues such as Met58, Thr270, Asp92, and Glu172, which contribute to its stability and orientation at the binding site. Hydrophobic contacts, such as those with residues Phe88 and Leu175, further stabilize the complex. The 2D and 3D interaction diagrams for GIV3727 with TAS2R4 outlined a well-defined binding mode characterized by strong hydrogen bonds and supportive hydrophobic interactions. These results indicate that GIV3727 might be a stable and effective ligand for TAS2R4 with important functional implications as a block

A)



B)

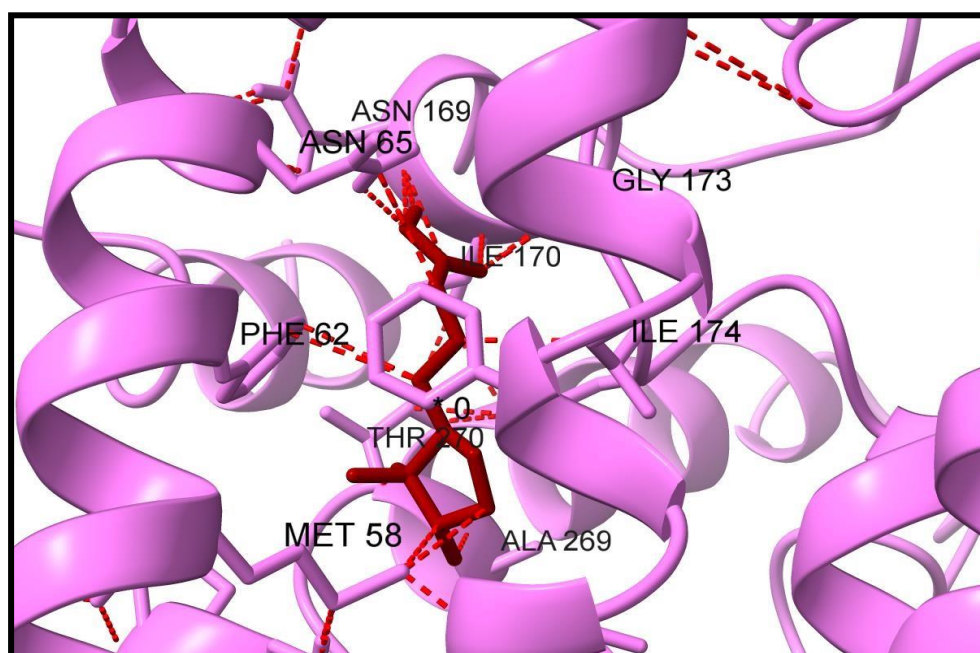


Figure 4.19: A) and B): 2D and 3D interaction pattern of GVI3727 ligand and TAS2R4 protein

4.9 Molecular Dynamic Simulations (MD) of Complexes Results

The docked complexes of TAS2R4 blockers were further taken for molecular dynamics simulation using the Desmond package of Schrödinger software. Three TAS2R4 complexes, BCML, GABA, GIV3727, have been selected for further MD simulation based on their pose analysis as shown in the figures below. The initial step involved energy minimization of the complex structure using the MMFF94S force field, followed by preprocessing at a physiological pH of 7.4. The OPLS3e force field was then used for simulation to accurately represent molecular interactions. The TAS2R4 complex was solved with the TIP3P water model inside a cubic water box, maintaining a 10 Å buffer zone around the protein atoms. The system was neutralized with Na⁺ and recalibrated at a concentration of 0.15 M within a 5 Å region. MD simulations were performed at a constant temperature of 303 K for 100 nanoseconds, allowing extensive analysis of protein-ligand interactions. Convergence of heavy atom (HA) counts to an RMSD of 0.3 ensured proper equilibration of the system. MD simulations were analyzed using the Simulation Interaction Diagram tool within the Desmond MD package. Simulation stability was monitored by tracking the RMSD of ligand and protein atom positions over time. RMSD analysis confirmed the stability of the protein-ligand complex during the simulation period. Additionally, hydrogen bond histograms were examined to identify the presence and stability of hydrogen bonds between proteins and ligands. This analysis revealed a large proportion of stable hydrogen bonds, indicating a strong interaction between TAS2R4 and the inhibitors. MD simulation results provided detailed insights into the dynamic behavior and stability of TAS2R4-ligand complexes, highlighting their potential utility as competitive inhibitors.

- **BCML Ligand Complex**

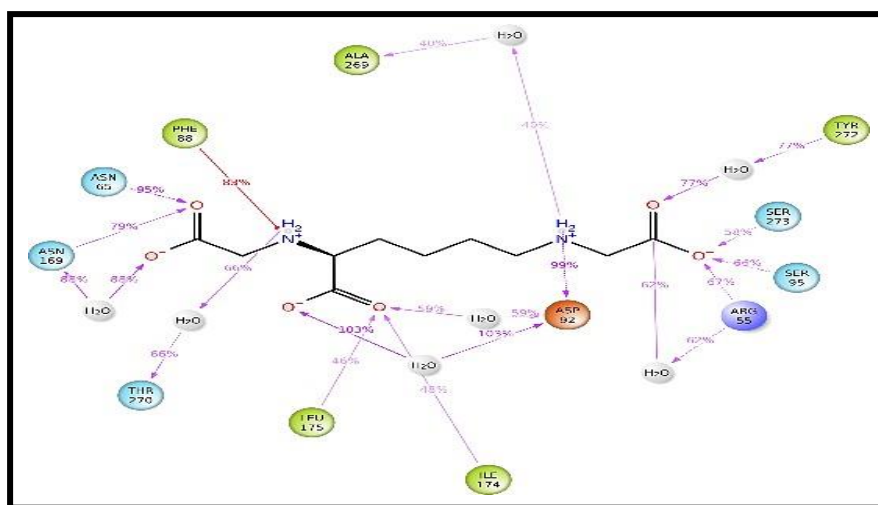


Figure 4.20: A) Shows protein-ligand contact after MD Simulation at 100ns.

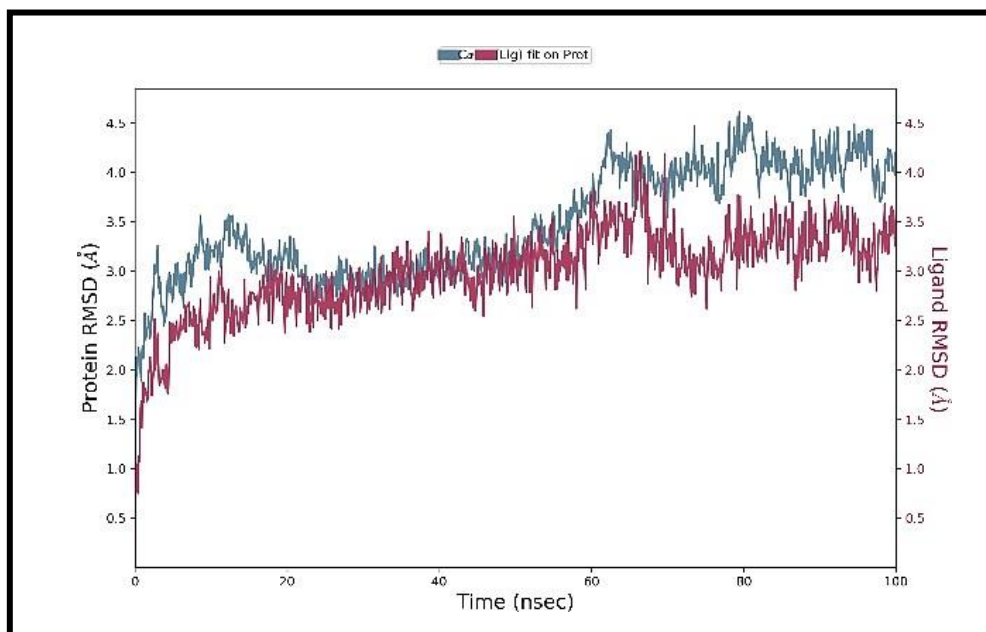


Figure 4.20: B) MD simulation of highly active, least active, and moderate compounds of BCML ligand complex. It explains RMSD profile of BCML ligand complex during simulations at 100ns. The RMSD (Root Mean Square Deviation) graph for the BCML protein and ligand complex shows the stability and conformational changes of both protein and ligand over a simulation time of 100 nanoseconds. The protein RMSD (blue line) initially increases and stabilizes around 3.0 to 4.0 Å, indicating that the protein reaches a relatively stable conformation after initial equilibrium. The ligand RMSD (red line) follows a similar trend, stabilizing around 2.5 to 3.5 Å, suggesting that the ligand remains permanently bound within the binding site while allowing some flexibility in the protein conformation and allowing adjustment. Overall, the graph indicates stable interactions between protein and ligand throughout the simulation.

- GABA Ligand Complex

A)

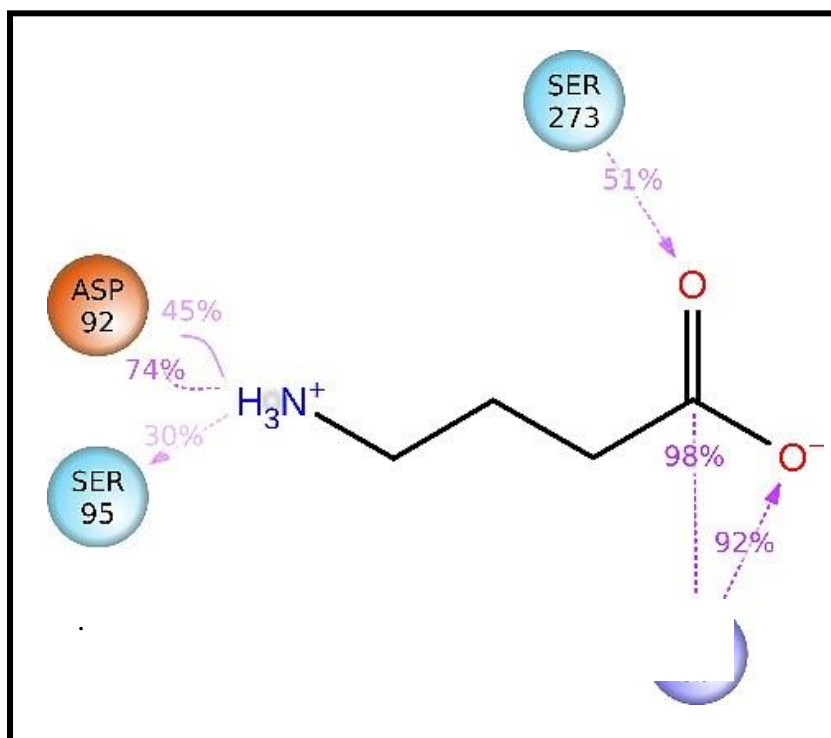


Figure 4.21: A) Shows protein-ligand contact after MD Simulation at 100ns

B)

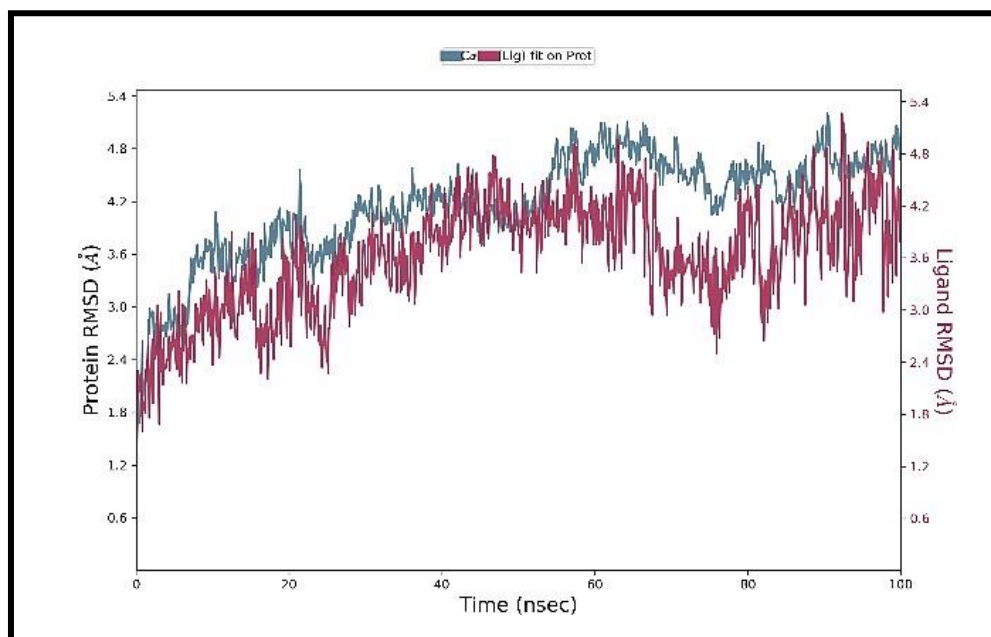


Figure 4.21: B) MD simulation of highly active, least active, and moderate compounds of GABA ligand complex. It explains RMSD profile of GABA ligand complex during simulations at 100ns. RMSD graph for GABA protein and ligand complex showing stability and conformational changes over a 100-nanosecond simulation period. The protein RMSD (blue line) shows an initial increase and stabilizes from about 3.5 to 4.8 Å, indicating that the protein acquires a stable conformation. The ligand RMSD (red line) follows a similar trend, stabilizing around 3.0 to 4.5 Å, suggesting that the ligand remains permanently bound within the binding site with some flexibility. Overall, the graph indicates stable interactions between the GABA protein and the ligand throughout the simulation.

- **GIV3727 Ligand Complex**

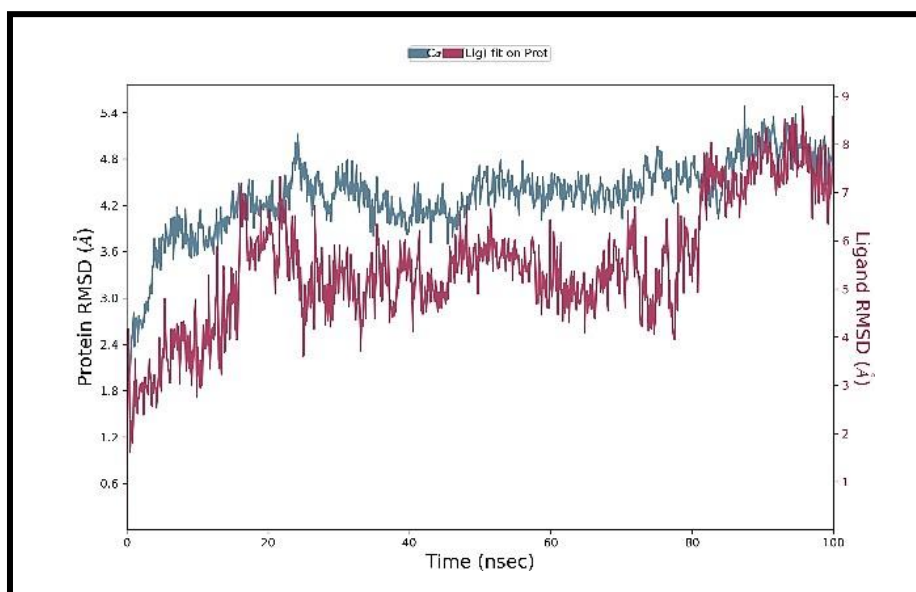
A) And B)

Figure 4.22: A) MD simulation of highly active, least active, and moderate compounds of GIV3727 ligand complex. It explains RMSD graph for GIV3727 protein and ligand complex showing stability and conformational changes over a 100 nanosecond simulation period. The protein RMSD (blue line) stabilizes from about 3.5 to 4.8 Å, indicating that the protein adopts a stable conformation. The ligand RMSD (red line) shows large fluctuations, which stabilize around 5.0 to 8.0 Å, indicating that when the ligand is bound, it exhibits significant flexibility and motion within the binding site. Overall, the graph indicates that the protein-ligand complex maintains a stable interaction, with the ligand exhibiting significant changes. B) Protein-ligand contact after MD simulation of 100ns.

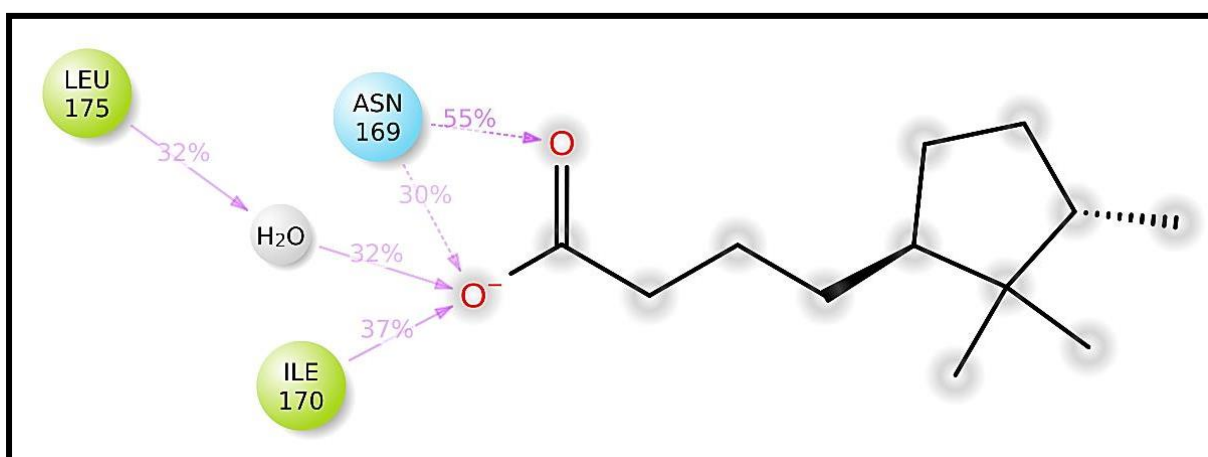


Figure 4.22: B) Shows protein-ligand contact after MD Simulation at 100ns.

Chapter 5: Conclusion and Future Perspective

Indeed, from the MD simulations and molecular docking studies, one can clearly show that this study has finally succeeded in clarifying the structural dynamics and interaction mechanisms between TAS2R4 and TAS2R14 as taste receptors. In this respect, these simulations have provided a comprehensive understanding of the stability and conformational flexibility of these receptors. MD simulations have long been particularly important, offering insight into how these receptors behave under physiological conditions. Molecular docking studies focus on predicting how small molecules, such as ligands, interact with these receptors. By identifying potential binding sites and using docking algorithms, these studies estimate how ligands orient within these sites and assess the stability of the resulting complexes through various scoring functions. This helps to understand how well ligands can bind and potentially affect receptor function, which is important for drug design or altering taste perception. MD simulations enabled to visualize the molecular dynamics of these taste receptors by placing them in a simulated environment. This involves setting the temperature of an appropriate aqueous environment and using molecular mechanics force fields to accurately model the physical and chemical interactions within and between proteins and ligands. The simulations trace atomic movements within the protein over time, revealing insights into its structural flexibility and stability. These computational approaches provide a detailed picture of how TAS2R4 and TAS2R14 receptors adapt and respond to their environment and interacting molecules, allowing for their potential in physiological and therapeutic contexts. Valuable insights into character are gained. This comprehensive analysis is important for designing compounds that can effectively target these receptors, enhancing or modifying taste perception for various applications. The dynamic stability of the protein-ligand complex was assessed through the RMSD and RMSF analyses. This was parallel to the Ramachandran plot assessment, which showed a high percentage of residues lying in favored regions, thus enabling the structural integrity of the models. The results from the molecular docking studies indicated, through key residue identification for TAS2R14 are Ile62, Phe76, Phe82, Leu85, Trp89, Ile179, Val180, Thr184, Ile187, Phe188, Phe243, Phe247, and Ile262 and for TAS2R4 are Leu159, Val160, Thr162, Arg163, Asn164, Phe168, Glu172, and Ser277 involved in ligand binding, a comparative analysis of the interaction patterns to increase our knowledge on ligand selectivity and receptor function. In addition, interaction analyses have identified specific amino acid residues playing important roles in the stabilization of the binding of ligands and provide valuable information toward the design of drugs and taste modulators in the future.

Computations that went into the study used MODELLER for homology modeling and ChimeraX for structure refinement, while using the Schrödinger suite both in MD simulations and docking, to provide an overall structure-based approach for G-protein coupled receptors study Demonstrated. Used here, this flexible approach ensured the production of results that are robust and reliable to the importance computational tools have in modern biochemical research. Moreover, correlation analysis between the docking scores and experimental data further validated the predictive accuracy of the computational models and hence their potential applications in real life. The study successfully identified five natural compounds as potential modulators of TAS2R4 and TAS2R14, demonstrating significant binding affinities. These findings provide a promising foundation for future therapeutic development targeting these taste receptors.

Future perspectives in this research come in when design of findings applies to a more effective flavor modulator; it may have important implications for both the food and pharmaceutical industries. Further studies could be made in the future to investigate other taste receptor mechanisms of interaction through similar computational methods that would increase the scope of research on taste modulation. This could increase the reliability of results and ultimately lead to new taste modifiers with higher efficacy, more appealing safety profiles, once the experimental validation is combined with computational predictions.

The development of these methods will, therefore, continue to pay off in sensory biology and could even open the road to innovative applications in taste perception and modulation. An even more exciting future avenue of research would be the ability to design taste modulators that are tailored to specific genetic profiles; this holds real potential for changing the approach toward taste disorders and variability in taste preferences.

References

- [1] I. W. Suryasa, M. Rodríguez-Gámez, and T. Koldoris, “Health and treatment of diabetes mellitus,” *Int. J. Health Sci.*, vol. 5, no. 1, pp. i–v, Apr. 2021, doi: 10.53730/ijhs.v5n1.2864.
- [2] K. C. Mekala and A. G. Bertoni, “Epidemiology of diabetes mellitus,” in *Transplantation, Bioengineering, and Regeneration of the Endocrine Pancreas*, Elsevier, 2020, pp. 49–58. doi: 10.1016/B978-0-12-814833-4.00004-6.
- [3] N. M. Avena, M. N. Potenza, and M. S. Gold, “Why Are We Consuming So Much Sugar Despite Knowing Too Much Can Harm Us?,” *JAMA Intern. Med.*, vol. 175, no. 1, p. 145, Jan. 2015, doi: 10.1001/jamainternmed.2014.6968.
- [4] H. Bahadar, S. Mostafalou, and M. Abdollahi, “Growing burden of diabetes in Pakistan and the possible role of arsenic and pesticides,” *J. Diabetes Metab. Disord.*, vol. 13, no. 1, p. 117, 2014, doi: 10.1186/s40200-014-0117-y.
- [5] S. Akhtar, J. A. Nasir, T. Abbas, and A. Sarwar, “Diabetes in Pakistan: A systematic review and meta-analysis,” *Pak. J. Med. Sci.*, vol. 35, no. 4, pp. 1173–1178, 2019, doi: 10.12669/pjms.35.4.194.
- [6] K. Świąder, K. Wegner, A. Piotrowska, F.-J. Tan, and A. Sadowska, “Plants as a source of natural high-intensity sweeteners: a review,” *J. Appl. Bot. Food Qual.*, pp. 160-171 Pages, Jun. 2019, doi: 10.5073/JABFQ.2019.092.022.
- [7] M. Barroso, L. Barros, M. Â. Rodrigues, M. J. Sousa, C. Santos-Buelga, and I. C. F. R. Ferreira, “Stevia rebaudiana Bertoni cultivated in Portugal: A prospective study of its antioxidant potential in different conservation conditions,” *Ind. Crops Prod.*, vol. 90, pp. 49–55, Nov. 2016, doi: 10.1016/j.indcrop.2016.06.013.
- [8] A. Forouzi, A. Ghasemnezhad, and R. G. Nasrabad, “Phytochemical response of Stevia plant to growth promoting microorganisms under salinity stress,” *South Afr. J. Bot.*, vol. 134, pp. 109–118, Nov. 2020, doi: 10.1016/j.sajb.2020.04.001.
- [9] G. Ferrazzano *et al.*, “Is Stevia rebaudiana Bertoni a Non Cariogenic Sweetener? A Review,” *Molecules*, vol. 21, no. 1, p. 38, Dec. 2015, doi: 10.3390/molecules21010038.
- [10] B. Arumugam, A. Subramaniam, and P. Alagaraj, “Stevia as a Natural Sweetener: A Review,” *Cardiovasc. Hematol. Agents Med. Chem.*, vol. 18, no. 2, pp. 94–103, Oct. 2020, doi: 10.2174/1871525718666200207105436.

References

- [11] D. P. Singh, M. Kumari, H. G. Prakash, G. P. Rao, and S. Solomon, "Phytochemical and Pharmacological Importance of Stevia: A Calorie-Free Natural Sweetener," *Sugar Tech*, vol. 21, no. 2, pp. 227–234, Apr. 2019, doi: 10.1007/s12355-019-00704-1.
- [12] A. K. Yadav, S. Singh, D. Dhyani, and P. S. Ahuja, "A review on the improvement of stevia [*Stevia rebaudiana* (Bertoni)]," *Can. J. Plant Sci.*, vol. 91, no. 1, pp. 1–27, Jan. 2011, doi: 10.4141/cjps10086.
- [13] A. M. Pierce-Feldmeyer, D. Josephson, A. Johnson, and R. Wieland, "Perception of Bitter Taste through Time-Intensity Measurements as Influenced by Taste Modulation Compounds in Steviol Glycoside Sweetened Beverages," *Beverages*, vol. 5, no. 3, p. 52, Aug. 2019, doi: 10.3390/beverages5030052.
- [14] S. A. Gravina, G. L. Yep, and M. Khan, "Human Biology of Taste," *Ann. Saudi Med.*, vol. 33, no. 3, pp. 217–222, May 2013, doi: 10.5144/0256-4947.2013.217.
- [15] J. Upadhyaya, N. Singh, R. P. Bhullar, and P. Chelikani, "The structure–function role of C-terminus in human bitter taste receptor T2R4 signaling," *Biochim. Biophys. Acta BBA - Biomembr.*, vol. 1848, no. 7, pp. 1502–1508, Jul. 2015, doi: 10.1016/j.bbamem.2015.03.035.
- [16] C. Hellfritsch, A. Brockhoff, F. Stähler, W. Meyerhof, and T. Hofmann, "Human Psychometric and Taste Receptor Responses to Steviol Glycosides," *J. Agric. Food Chem.*, vol. 60, no. 27, pp. 6782–6793, Jul. 2012, doi: 10.1021/jf301297n.
- [17] R. Singla and V. Jaitak, "Synthesis of rebaudioside A from stevioside and their interaction model with hTAS2R4 bitter taste receptor," *Phytochemistry*, vol. 125, pp. 106–111, May 2016, doi: 10.1016/j.phytochem.2016.03.004.
- [18] M. Haque, J. McKimm, M. Sartelli, N. Samad, S. Z. Haque, and M. A. Bakar, "A narrative review of the effects of sugar-sweetened beverages on human health: A key global health issue," *J. Popul. Ther. Clin. Pharmacol.*, vol. 27, no. 1, pp. e76–e103, Mar. 2020, doi: 10.15586/jptcp.v27i1.666.
- [19] S. Kumar, P. K. Tyagi, D. Gola, A. K. Mishra, and A. Arya, "Plant-Based Sweeteners and Their Applications in Modern Lifestyle," in *Non-Timber Forest Products*, A. Husen, R. K. Bachheti, and A. Bachheti, Eds., Cham: Springer International Publishing, 2021, pp. 75–103. doi: 10.1007/978-3-030-73077-2_4.
- [20] G. E. Inglett, "A history of sweeteners-natural and synthetic," *J. Toxicol. Environ. Health*, vol. 2, no. 1, pp. 207–214, Sep. 1976, doi: 10.1080/15287397609529427.

References

- [21] G. Negri and R. Tabach, "Saponins, tannins and flavonols found in hydroethanolic extract from *Periandra dulcis* roots," *Rev. Bras. Farmacogn.*, vol. 23, no. 6, pp. 851–860, Nov. 2013, doi: 10.1590/S0102-695X2013000600001.
- [22] M. Puri, D. Sharma, and C. J. Barrow, "Enzyme-assisted extraction of bioactives from plants," *Trends Biotechnol.*, vol. 30, no. 1, pp. 37–44, Jan. 2012, doi: 10.1016/j.tibtech.2011.06.014.
- [23] J. Ahmad, I. Khan, R. Blundell, J. Azzopardi, and M. F. Mahomoodally, "Stevia rebaudiana Bertoni.: an updated review of its health benefits, industrial applications and safety," *Trends Food Sci. Technol.*, vol. 100, pp. 177–189, Jun. 2020, doi: 10.1016/j.tifs.2020.04.030.
- [24] A. A. Momtazi-Borojeni, S.-A. Esmaeili, E. Abdollahi, and A. Sahebkar, "A Review on the Pharmacology and Toxicology of Steviol Glycosides Extracted from *Stevia rebaudiana*," *Curr. Pharm. Des.*, vol. 23, no. 11, pp. 1616–1622, May 2017, doi: 10.2174/1381612822666161021142835.
- [25] School of Agriculture and Rural Development, Bangladesh Open University, Gazipur - 1705, Bangladesh *et al.*, "Cultivation and uses of stevia (*Stevia rebaudiana bertoni*): A review," *Afr. J. FOOD Agric. Nutr. Dev.*, vol. 17, no. 04, pp. 12745–12757, Nov. 2017, doi: 10.18697/ajfand.80.16595.
- [26] N. Kumari, R. C. Ranac, Y. P. Sharma, and S. Kumar, "Extraction, Purification and Analysis of Sweet Compounds in *Stevia rebaudiana Bertoni* using Chromatographic Techniques," *Indian J. Pharm. Sci.*, vol. 79, no. 4, 2017, doi: 10.4172/pharmaceutical-sciences.1000270.
- [27] Verónica López-Carbón *et al.*, "Simple and Efficient Green Extraction of Steviol Glycosides from *Stevia rebaudiana* Leaves".
- [28] M. V. S. De Andrade, S. R. Lucho, R. D. De Castro, and P. R. Ribeiro, "Alternative for natural sweeteners: Improving the use of stevia as a source of steviol glycosides," *Ind. Crops Prod.*, vol. 208, p. 117801, Feb. 2024, doi: 10.1016/j.indcrop.2023.117801.
- [29] C. Dawid, C. Well, A. Brockhoff, F. Stähler, W. Meyerhof, and T. Hofmann, "Molecular Determinants of the Bittersweet Janus Head of Steviol Glycosides from *Stevia rebaudiana* (Bert.) Bertoni," in *ACS Symposium Series*, vol. 1191, B. Guthrie, J. Beauchamp, A. Buettner, and B. K. Lavine, Eds., Washington, DC: American Chemical Society, 2015, pp. 197–207. doi: 10.1021/bk-2015-1191.ch015.

References

- [30] V. Bhardwaj, R. Singh, P. Singh, R. Purohit, and S. Kumar, “Elimination of bitter-off taste of stevioside through structure modification and computational interventions,” *J. Theor. Biol.*, vol. 486, p. 110094, Feb. 2020, doi: 10.1016/j.jtbi.2019.110094.
- [31] P. Lu, C.-H. Zhang, L. M. Lifshitz, and R. ZhuGe, “Extraoral bitter taste receptors in health and disease,” *J. Gen. Physiol.*, vol. 149, no. 2, pp. 181–197, Feb. 2017, doi: 10.1085/jgp.201611637.
- [32] S. Prasad Pydi, N. Singh, J. Upadhyaya, R. Pal Bhullar, and P. Chelikani, “The third intracellular loop plays a critical role in bitter taste receptor activation,” *Biochim. Biophys. Acta BBA - Biomembr.*, vol. 1838, no. 1, pp. 231–236, Jan. 2014, doi: 10.1016/j.bbamem.2013.08.009.
- [33] Moon Young Yang, “Predicted structure of fully activated human bitter taste receptor TAS2R4 complexed with G protein and agonists”.
- [34] M. Behrens, S. Foerster, F. Staehler, J.-D. Raguse, and W. Meyerhof, “Gustatory Expression Pattern of the Human TAS2R Bitter Receptor Gene Family Reveals a Heterogenous Population of Bitter Responsive Taste Receptor Cells,” *J. Neurosci.*, vol. 27, no. 46, pp. 12630–12640, Nov. 2007, doi: 10.1523/JNEUROSCI.1168-07.2007.
- [35] W. Meyerhof *et al.*, “The Molecular Receptive Ranges of Human TAS2R Bitter Taste Receptors,” *Chem. Senses*, vol. 35, no. 2, pp. 157–170, Feb. 2010, doi: 10.1093/chemse/bjp092.
- [36] G. De León, E. Fröhlich, and S. Salar-Behzadi, “Bitter taste in silico: A review on virtual ligand screening and characterization methods for TAS2R-bitterant interactions,” *Int. J. Pharm.*, vol. 600, p. 120486, May 2021, doi: 10.1016/j.ijpharm.2021.120486.
- [37] O. A. Arodola, S. Kanchi, P. Hloma, K. Bisetty, A. M. Asiri, and Inamuddin, “An in-silico layer-by-layer adsorption study of the interaction between Rebaudioside A and the T1R2 human sweet taste receptor: modelling and biosensing perspectives,” *Sci. Rep.*, vol. 10, no. 1, p. 18391, Oct. 2020, doi: 10.1038/s41598-020-75123-4.
- [38] H. Unal and S. S. Karnik, “Domain coupling in GPCRs: the engine for induced conformational changes,” *Trends Pharmacol. Sci.*, vol. 33, no. 2, pp. 79–88, Feb. 2012, doi: 10.1016/j.tips.2011.09.007.
- [39] M. Masamoto, Y. Mitoh, M. Kobashi, N. Shigemura, and R. Yoshida, “Effects of bitter receptor antagonists on behavioral lick responses of mice,” *Neurosci. Lett.*, vol. 730, p. 135041, Jun. 2020, doi: 10.1016/j.neulet.2020.135041.

References

- [40] S. P. Pydi *et al.*, “Abscisic Acid Acts as a Blocker of the Bitter Taste G Protein-Coupled Receptor T2R4,” *Biochemistry*, vol. 54, no. 16, pp. 2622–2631, Apr. 2015, doi: 10.1021/acs.biochem.5b00265.
- [41] J. P. Slack *et al.*, “Modulation of Bitter Taste Perception by a Small Molecule hTAS2R Antagonist,” *Curr. Biol.*, vol. 20, no. 12, pp. 1104–1109, Jun. 2010, doi: 10.1016/j.cub.2010.04.043.
- [42] W. S. U. Roland *et al.*, “6-Methoxyflavanones as Bitter Taste Receptor Blockers for hTAS2R39,” *PLoS ONE*, vol. 9, no. 4, p. e94451, Apr. 2014, doi: 10.1371/journal.pone.0094451.
- [43] B. Webb and A. Sali, “Comparative Protein Structure Modeling Using MODELLER,” *Curr. Protoc. Bioinforma.*, vol. 54, no. 1, Jun. 2016, doi: 10.1002/cpbi.3.
- [44] The UniProt Consortium, “UniProt: a hub for protein information,” *Nucleic Acids Res.*, vol. 43, no. D1, pp. D204–D212, Jan. 2015, doi: 10.1093/nar/gku989.
- [45] T. Claff *et al.*, “Single Stabilizing Point Mutation Enables High-Resolution Co-Crystal Structures of the Adenosine A_{2A} Receptor with Preladenant Conjugates,” *Angew. Chem. Int. Ed.*, vol. 61, no. 22, p. e202115545, May 2022, doi: 10.1002/anie.202115545.
- [46] I.-J. Chen and N. Foloppe, “Conformational Sampling of Druglike Molecules with MOE and Catalyst: Implications for Pharmacophore Modeling and Virtual Screening,” *J. Chem. Inf. Model.*, vol. 48, no. 9, pp. 1773–1791, Sep. 2008, doi: 10.1021/ci800130k.
- [47] S. Vijayakumar and S. Rajalakshmi, “Exploring novel natural compound inhibitors for Parkinsonian receptor (DJ1) by homology modeling, molecular docking and MD simulations,” *Vegetos*, vol. 34, no. 4, pp. 959–970, Dec. 2021, doi: 10.1007/s42535-021-00263-5.
- [48] A. Waterhouse *et al.*, “SWISS-MODEL: homology modelling of protein structures and complexes,” *Nucleic Acids Res.*, vol. 46, no. W1, pp. W296–W303, Jul. 2018, doi: 10.1093/nar/gky427.
- [49] M. L. Verdonk, J. C. Cole, M. J. Hartshorn, C. W. Murray, and R. D. Taylor, “Improved protein–ligand docking using GOLD,” *Proteins Struct. Funct. Bioinforma.*, vol. 52, no. 4, pp. 609–623, Sep. 2003, doi: 10.1002/prot.10465.
- [50] Y. Kim *et al.*, “Bitter taste receptor activation by cholesterol and an intracellular tastant,” *Nature*, vol. 628, no. 8008, pp. 664–671, Apr. 2024, doi: 10.1038/s41586-024-07253-y.
- [51] T. Claff *et al.*, “Single Stabilizing Point Mutation Enables High-Resolution Co-Crystal Structures of the Adenosine A_{2A} Receptor with Preladenant Conjugates,” *Angew. Chem. Int. Ed.*, vol. 61, no. 22, p. e202115545, May 2022, doi: 10.1002/anie.202115545.

References

- [52] T. Seidel, S. D. Bryant, G. Ibis, G. Poli, and T. Langer, “3D Pharmacophore Modeling Techniques in Computer-Aided Molecular Design Using LigandScout,” in *Tutorials in Chemoinformatics*, 1st ed., A. Varnek, Ed., Wiley, 2017, pp. 279–309. doi: 10.1002/9781119161110.ch20.
- [53] S. P. Pydi, T. Sobotkiewicz, R. Billakanti, R. P. Bhullar, M. C. Loewen, and P. Chelikani, “Amino Acid Derivatives as Bitter Taste Receptor (T2R) Blockers,” *J. Biol. Chem.*, vol. 289, no. 36, pp. 25054–25066, Sep. 2014, doi: 10.1074/jbc.M114.576975.
- [54] GOLD SUIT, <https://gold-suite.software.informer.com/>.
- [55] M. Y. Yang, A. Mafi, S.-K. Kim, W. A. Goddard, and B. Guthrie, “Predicted structure of fully activated human bitter taste receptor TAS2R4 complexed with G protein and agonists,” *QRB Discov.*, vol. 2, p. e3, 2021, doi: 10.1017/qrd.2021.1.

Appendix

Appendix

Molecule	IC50(n	IC50(
ChEMBL ID	Smiles	m)	M)	PIC50
CHEMBL393 0803	<chem>Cc1ccc(S(=O)(=O)N(Cc2ccc(F)cc2)CC2CCC(C(=O)O)CC2)cc1</chem>	83	0.0000 00083	7.0809 2191
CHEMBL392 9345	<chem>COc1ccc(CN(Cc2ccc(OC)cc2)S(=O)(=O)c2ccc(C(=O)O)cc2)cc1</chem>	4140	0.0000 0414	5.3829 9966
CHEMBL394 5665	<chem>Cn1c(=O)c2cc(S(=O)(=O)Nc3ccc4c(c3)OCCO4)ccc2n(C)c1=O</chem>	706	0.0000 00706	6.1511 953
CHEMBL397 3557	<chem>Cn1c(=O)c(=O)n(C)c2cc(S(=O)(=O)Nc3ccc(Cc4ccc4)cc3)ccc21</chem>	6140	0.0000 0614	5.2118 3163
CHEMBL149 9181	<chem>CCc1nc(SCC(=O)N2CCC(C)CC2)c2c(=O)n(C)c(=O)n(C)c2n1</chem>	721	0.0000 00721	6.1420 6474
CHEMBL395 4153	<chem>COc1cccc(CN(Cc2ccc(C(=O)O)cc2)S(=O)(=O)c2cccc2)c1</chem>	345	0.0000 00345	6.4621 809
CHEMBL390 7800	<chem>Nc1ccc(S(=O)(=O)N(Cc2ccc(F)cc2)CC2CCC(C(=O)O)CC2)cc1</chem>	1651	0.0000 01651	5.7822 5293
CHEMBL389 3065	<chem>O=C(O)c1ccc(S(=O)(=O)N(Cc2cccc2)Cc2ccc(Cl)cc2)cc1</chem>	3977	0.0000 03977	5.4004 4441
CHEMBL398 2311	<chem>CSc1ccc(CN(Cc2cccc2)S(=O)(=O)c2ccc(C(=O)O)cc2)cc1</chem>	2458	0.0000 02458	5.6094 1812
CHEMBL309 2287	<chem>COc1ccc(CN(Cc2cccc2)S(=O)(=O)c2ccc(C(=O)O)cc2)cc1</chem>	200	0.0000 002	6.6989 7
CHEMBL396 2533	<chem>O=C(O)c1ccc(S(=O)(=O)N(Cc2cccc2)Cc2cccc2F)cc1</chem>	6164	0.0000 06164	5.2101 3737
CHEMBL394 4915	<chem>COc1ccc(OC)c(/C=C2\SC(=S)N(CCC(=O)O)C2=O)c1</chem>	2750	0.0000 0275	5.5606 6731
CHEMBL187 0906	<chem>CCN(C(=O)CN(C)S(=O)(=O)c1ccc2c(c1)n(C)c(=O)c(=O)n2C)c1cccc(C)c1</chem>	14926	0.0000 14926	4.8260 5656
CHEMBL395 6466	<chem>COc1ccc2c(c1)C(c1cccc1)N(S(=O)(=O)c1ccc(C(=O)O)cc1)CC2</chem>	2879	0.0000 02879	5.5407 5834
CHEMBL398 3085	<chem>COc1ccc(CN(Cc2ccc(OC)c(F)c2)S(=O)(=O)c2ccc(C(=O)O)cc2)cc1</chem>	1110	0.0000 0111	5.9546 7702

Appendix

CHEMBL392	COc1cccc1CN(Cc1ccc(C(=O)O)cc1)S(=O)(=O)c	0.0000	5.5917	
9937	1ccc(O)cc1	2560	0256	6003
CHEMBL390	COc1cccc(CN(Cc2ccc(C(=O)O)cc2)S(=O)(=O)c2	0.0000	6.7258	
1989	ccc(O)cc2)c1	188	00188	4215
CHEMBL390	O=C(O)c1ccc(S(=O)(=O)N(Cc2ccccc2)Cc2cccc(F	0.0000	5.6363	
8873)c2)cc1	2310	0231	8802
CHEMBL389	O=C(O)c1ccc(S(=O)(=O)N(Cc2ccccc2)Cc2ccccc2	0.0000	5.3481	
9828	Cl)cc1	4486	04486	4073
CHEMBL391	COc1ccc(CN(C2CCc3ccccc32)S(=O)(=O)c2ccc(0.0000	5.6170	
6083	C(=O)O)cc2)cc1	2415	02415	8286
CHEMBL398	COc1cccc1CN(Cc1ccc(C(=O)O)cc1)S(=O)(=O)c	0.0000	5.8880	
2834	1cccc1	1294	01294	6572
CHEMBL393	O=C(O)c1ccc(S(=O)(=O)N(Cc2ccccc2)Cc2ccco2)	0.0000	5.3372	
2685	cc1	4600	046	4217
CHEMBL397	COc1ccc(CN(Cc2ccccc2)S(=O)(=O)c2ccc(C(=O)	0.0000	6.1687	
8302	O)cc2)cc1OC	678	00678	7031
CHEMBL397	CC(=O)Nc1ccc(S(=O)(=O)N(Cc2ccc(F)cc2)CC2C	0.0000	6.0746	
6205	CC(C(=O)O)CC2)cc1	842	00842	8791
CHEMBL395	CC(=O)CSc1nc(C2CCCC2)nc2c1c(=O)n(C)c(=O)	0.0000	5.2653	
5017	n2C	5428	05428	6016
CHEMBL396	CCN(Cc1ccc(OC)cc1)S(=O)(=O)c1ccc(C(=O)O)c	0.0000		
5320	c1	10000	1	5
CHEMBL393	COc1ccc(CN(Cc2cccc(Cl)c2)S(=O)(=O)c2ccc(C(0.0000	5.7258	
1998	=O)O)cc2)cc1	1880	0188	4215
CHEMBL152	O=C(O)c1ccc(S(=O)(=O)N(Cc2ccccc2)Cc2ccccc2	0.0000	5.1112	
3162)cc1	7740	0774	5904
CHEMBL394	COc1ccc(CN(Cc2ccc(C(=O)O)cc2)S(=O)(=O)c2c	0.0000	5.4647	
7157	cc(O)cc2)cc1	3430	0343	0588
CHEMBL390	COc1ccc(CN(Cc2cc(OC)cc(OC)c2)S(=O)(=O)c2c	0.0000	4.9157	
2821	cc(C(=O)O)cc2)cc1	12141	12141	4554
CHEMBL389	Cc1cccc(CN(Cc2ccccc2)S(=O)(=O)c2ccc(C(=O)O	0.0000	5.6401	
4410)cc2)c1	2290	0229	6452
CHEMBL396	N#Cc1ccc(CN(Cc2ccccc2)S(=O)(=O)c2ccc(C(=O)	0.0000	5.7332	
2098)O)cc2)cc1	1848	01848	9803
CHEMBL143	CCOC(=O)C1CCC(CN(Cc2ccccc2)S(=O)(=O)c2c	0.0000	5.6300	
4982	cc(Br)cc2)CC1	2344	02344	4239

Appendix

CHEMBL390 9546	<chem>COc1cccc(CN(CC2CCC(C(=O)O)CC2)S(=O)(=O)c2ccc(C)cc2)c1</chem>	36	00036	7.4436 975
CHEMBL396 2410	<chem>O=C(O)c1ccc(CN(Cc2ccc(F)cc2)S(=O)(=O)c2ccc(O)cc2)cc1</chem>	4086	04086	5.3887 0164
CHEMBL393 5097	<chem>Cc1ccccc1NS(=O)(=O)c1ccc2c(c1)c(=O)n(C)c(=O)n2C</chem>	1726	01726	5.7629 5921
CHEMBL392 0736	<chem>COc1cc(/C=C2\SC(=S)N(CCC(=O)O)C2=O)cc(O)C)c1</chem>	5378	05378	5.2693 792
CHEMBL391 1317	<chem>Cn1c(=O)c2cc(S(=O)(=O)NC3CCCCC3)ccc2n(C)c1=O</chem>	7239	07239	5.1403 2142
CHEMBL393 8203	<chem>Cn1c(=O)c2cc(S(=O)(=O)Nc3ccc(Cl)cc3F)ccc2n(C)c1=O</chem>	9703	09703	5.0130 9397
CHEMBL390 9212	<chem>O=C(O)C1CCC(CN(Cc2ccc(F)cc2)S(=O)(=O)Cc2cccc2)CC1</chem>	9570	0957	5.0190 8806
CHEMBL393 7130	<chem>COc1ccc(CN(Cc2ccccc2C#N)S(=O)(=O)c2ccc(C(=O)O)cc2)cc1</chem>	4610	0461	5.3362 9907
CHEMBL389 1588	<chem>O=C(O)c1ccc(S(=O)(=O)N(Cc2ccccc2)Cc2ccc(O)cc2)cc1</chem>	5207	05207	5.2834 1242
CHEMBL132 6627	<chem>COc1ccc(CN(CC2CCC(C(=O)O)CC2)C(=S)Nc2cccc2OC)cc1</chem>	8852	08852	5.0529 5859
CHEMBL390 4387	<chem>Cc1ccc(CN(CC2CCC(C(=O)O)CC2)S(=O)(=O)c2ccc(C)cc2)cc1</chem>	109	00109	6.9625 735
CHEMBL391 6808	<chem>O=C(O)c1ccc(CN(Cc2ccc(F)cc2)S(=O)(=O)c2ccc(cc2)cc1</chem>	935	00935	6.0291 8839
CHEMBL390 8011	<chem>N#C/C(=C\c1ccc(O)C(=O)Nc1nnc(-c2ccccc2)s1</chem>	499	00499	6.3018 9945
CHEMBL395 3366	<chem>CCN(C)C(=O)CSc1nc(C)nc2c1c(=O)n(C)c(=O)n2C</chem>	861	00861	6.0649 9685
CHEMBL396 2122	<chem>Cc1nc(SCC(=O)N2CCCCC2)c2c(=O)n(C)c(=O)n(C)c2n1</chem>	292	00292	6.5346 1715
CHEMBL171 1155	<chem>CCOC(=O)N1CCN(C(=O)CSc2nc(CC)nc3c2c(=O)n(C)c(=O)n3C)CC1</chem>	763	00763	6.1174 7546
CHEMBL398 2886	<chem>Cc1ccc(S(=O)(=O)N(Cc2ccc(C#N)cc2)CC2CCC(C(=O)O)CC2)cc1</chem>	499	00499	6.3018 9945
CHEMBL136 6449	<chem>Cc1nc(SCC(=O)N2CCOCC2)c2c(=O)n(C)c(=O)n(C)c2n1</chem>	1006	01006	5.9974 0202

Appendix

CHEMBL391 7592	CCOC(=O)C1CCC(CN(Cc2ccccc2)S(=O)(=O)c2c cc(NC(C)=O)cc2)CC1	334	00334	5353	0.0000	6.4762
CHEMBL389 5501	Cc1cc(C)c(C#N)c(NS(=O)(=O)c2ccc3c(c2)c(=O)n (C)c(=O)n3C)c1	1946	01946	5716	0.0000	5.7108
CHEMBL395 4532	CC(C)CN(CC(C)C)S(=O)(=O)c1ccc(C(=O)O)cc1	15000	15	0874	0.0000	4.8239
CHEMBL393 0424	COc1ccc(CN(Cc2ccc(F)cc2)S(=O)(=O)c2ccc(C(= O)O)cc2)cc1	1970	0197	3377	0.0000	5.7055
CHEMBL390 7115	O=C(O)c1ccc(S(=O)(=O)N(Cc2ccccc2)Cc2ccc3c(c2)OCO3)cc1	2167	02167	4109	0.0000	5.6641
CHEMBL390 2826	COc1ccc(CN(CCc2ccccc2)S(=O)(=O)c2ccc(C(=O)O)cc2)cc1	4580	0458	3452	0.0000	5.3391
CHEMBL389 2139	COc1ccc(C2Cc3ccccc3CN2S(=O)(=O)c2ccc(C(= O)O)cc2)cc1	6267	06267	4031	0.0000	5.2029
CHEMBL395 2516	COc1ccc(CN(Cc2ccccc2)S(=O)(=O)c2ccc(- c3nn[nH]n3)cc2)cc1	3670	0367	3394	0.0000	5.4353
CHEMBL397 8325	COc1ccc(CN(Cc2ccc(C(=O)O)cc2)S(=O)(=O)c2c cccc2)cc1	2219	02219	427	0.0000	5.6538
CHEMBL389 2212	COc1ccc(CN(Cc2ccccc2OC)S(=O)(=O)c2ccc(C(= O)O)cc2)cc1	2943	02943	0974	0.0000	5.5312
CHEMBL396 1709	COc1ccc(CN(Cc2ccccc2)S(=O)(=O)c2ccc(C(=O) O)cc2)en1	3258	03258	4892	0.0000	5.4870
CHEMBL389 3863	CCCN(Cc1ccc(OC)cc1)S(=O)(=O)c1ccc(C(=O)O) cc1	3750	0375	6873	0.0000	5.4259
CHEMBL391 6784	COc1ccc(CN(Cc2ccc(OC)c(OC)c2)S(=O)(=O)c2c cc(C(=O)O)cc2)cc1	1470	0147	8267	0.0000	5.8326
CHEMBL391 2878	Cc1ccc(CN(Cc2ccccc2)S(=O)(=O)c2ccc(C(=O)O) cc2)cc1	5394	05394	8906	0.0000	5.2680
CHEMBL393 2940	O=C(O)c1ccc(S(=O)(=O)N(Cc2ccccc2)Cc2ccc(F) cc2)cc1	8283	08283	1234	0.0000	5.0818
CHEMBL393 1168	COc1ccc(CN(Cc2ccc(OC)c2)S(=O)(=O)c2ccc(C(=O)O)cc2)cc1	2460	0246	6489	0.0000	5.6090
CHEMBL394 6037	COc1ccc(CN(Cc2ccc(F)c(OC)c2)S(=O)(=O)c2ccc (C(=O)O)cc2)cc1	1650	0165	1606	0.0000	5.7825
CHEMBL392 5369	COc1ccc(CN(Cc2ccccc2Cl)S(=O)(=O)c2ccc(C(= O)O)cc2)cc1	7044	07044	8065	0.0000	5.1521

Appendix

CHEMBL393 0424	COc1ccc(CN(Cc2ccc(F)cc2)S(=O)(=O)c2ccc(C(=O)O)cc2)cc1	8283	0.0000	5.0818	08283	1234
CHEMBL394 0903	COc1ccc(CN(Cc2ccc(F)cc2F)S(=O)(=O)c2ccc(C(=O)O)cc2)cc1	1255	0.0000	5.9013	01255	5627
CHEMBL398 0504	N#C/C(=C\c1ccc2c(c1)OCO2)C(=O)Nc1nnc(-c2ccccc2)s1	2906	0.0000	5.5367	02906	0439
CHEMBL394 8049	Cc1nc2ccc(NS(=O)(=O)c3ccc4c(c3)n(C)c(=O)c(=O)n4C)cc2nc1C	6332	0.0000	5.1984	06332	5909
CHEMBL331 1308	COc1ccc(S(=O)(=O)Nc2c(C)cc(C)cc2C)cc1	39810.7 2	3.9810 7E-05	4.3999 9997		
CHEMBL395 4619	COc1cccc(CN(Cc2ccccc2)S(=O)(=O)c2ccc(C(=O)O)cc2)c1	5991	0.0000	5.2225	05991	0068
CHEMBL397 0253	N#Cc1cccc1CN(Cc1cccc1)S(=O)(=O)c1ccc(C(=O)O)cc1	4627	0.0000	5.3347	04627	005
CHEMBL391 1496	O=C(O)C1CCC(CN(Cc2ccc(F)cc2)S(=O)(=O)c2cccnc2)CC1	8434	0.0000	5.0739	08434	664
CHEMBL395 2395	O=C(O)c1ccc(S(=O)(=O)N(Cc2ccccc2)Cc2ccccc(C)l)c2)cc1	4286	0.0000	5.3679	04286	4783
CHEMBL389 2708	COc1ccc(CN(Cc2ccccc2)S(=O)(=O)c2ccc(C(=O)O)cc2)cc1C	1995	0.0000	5.7000	01995	571
CHEMBL388 9984	COc1ccc(CN(Cc2ccccc2)S(=O)(=O)c2cccc(OC)c2)cc1	2219	0.0000	5.6538	02219	427
CHEMBL397 7716	COc1ccc(CN(C(C)c2ccccc2)S(=O)(=O)c2ccc(C(=O)O)cc2)cc1	1397	0.0000	5.8548	01397	0359
CHEMBL398 0678	Cc1cc(NC(=S)N(Cc2ccccc2C)CC2CCC(C(=O)O)O)CC2)ccc1Cl	4872	0.0000	5.3122	04872	9272
CHEMBL397 2175	O=C(O)C1CCC(CN(Cc2ccc(F)cc2)S(=O)(=O)c2ccc(O)cc2)CC1	342	0.0000	6.4659	00342	7389
CHEMBL389 2321	O=C(O)c1ccc(CN(Cc2ccc(F)c2)S(=O)(=O)c2ccc(O)cc2)cc1	406	0.0000	6.3914	00406	7397
CHEMBL390 0023	CCOC(=O)C1CCC(CN(Cc2ccc(Br)c2)S(=O)(=O)c2ccc3c(c2)OCCO3)CC1	2567	0.0000	5.5905	02567	7413
CHEMBL390 5445	COc1ccc(S(=O)(=O)N(Cc2ccc(F)cc2)CC2CCC(C(=O)O)CC2)cc1	92	0.0000	7.0362	00092	1217
CHEMBL396 4825	COc1ccc2c(c1)CCN(S(=O)(=O)c1ccc(C(=O)O)cc1)C2c1ccccc1	9616	0.0000	5.0170	09616	0555

Appendix

CHEMBL150 3512	<chem>Cn1c(=O)c(=O)n(C)c2cc(S(=O)(=O)Nc3ccc4c(c3)OCCO4)ccc21</chem>	7710	0771	4562	0.0000	5.1129
CHEMBL140 1915	<chem>Cn1c(=O)c2cc(S(=O)(=O)Nc3ccc4c(c3)OCO4)ccc2n(C)c1=O</chem>	264	00264	9607	0.0000	6.5783
CHEMBL141 9634	<chem>Cc1c(F)cccc1NS(=O)(=O)c1ccc2c(c1)c(=O)n(C)c(=O)n2C</chem>	935	00935	8839	0.0000	6.0291
CHEMBL397 0702	<chem>CNS(=O)(=O)c1ccc2[nH]c(=O)c(=O)[nH]c2c1</chem>	6234	06234	332	0.0000	5.2052
CHEMBL309 2263	<chem>COc1ccc(CN(CC2CCCC2)S(=O)(=O)c2ccc(C(=O)O)cc2)cc1</chem>	3470	0347	7053	0.0000	5.4596
CHEMBL397 6457	<chem>O=C(O)c1ccc(CN(Cc2cccc(F)c2)S(=O)(=O)c2ccc(O)cc2)cc1</chem>	459	00459	8731	0.0000	6.3381
CHEMBL398 6131	<chem>COc1cccc1CN(Cc1cccc1)S(=O)(=O)c1ccc(C(=O)O)cc1</chem>	5061	05061	6366	0.0000	5.2957
CHEMBL398 4415	<chem>CCc1ccc(CN(Cc2cccc2)S(=O)(=O)c2ccc(C(=O)O)cc2)cc1</chem>	8580	0858	1271	0.0000	5.0665
CHEMBL390 7807	<chem>O=C(O)c1ccc(CN(Cc2cccc2F)S(=O)(=O)c2cccc2)cc1</chem>	429	00429	4271	0.0000	6.3675
CHEMBL390 2438	<chem>COc1ccc2c(c1)-c1cccc1CN(S(=O)(=O)c1ccc(C(=O)O)cc1)C2</chem>	3571	03571	1015	0.0000	5.4472
CHEMBL139 5308	<chem>Cc1cc2c(cc1S(=O)(=O)Nc1ccc(F)cc1)n(C)c(=O)c(=O)n2C</chem>	12623	12623	3742	0.0000	4.8988
CHEMBL394 8525	<chem>COc1cc(OC)c(/C=C2\SC(=S)N(CCC(=O)O)C2=O)c(OC)c1</chem>	9371	09371	1406	0.0000	5.0282
CHEMBL397 9438	<chem>Cn1c(=O)c2c(SCC(=O)N3CCCCC3)ccnc2n(C)c1=O</chem>	2377	02377	7082	0.0000	5.6239
CHEMBL392 1682	<chem>CC(=O)Nc1ccc(S(=O)(=O)N(Cc2cccc2)CC2CC(C(C(=O)O)CC2)cc1</chem>	1619	01619	5315	0.0000	5.7907
CHEMBL393 8183	<chem>CCOc1ccc(CN(Cc2ccco2)S(=O)(=O)c2ccc(C(=O)O)cc2)cc1</chem>	3000	03	7875	0.0000	5.5228
CHEMBL391 3926	<chem>COc1cc(OC)c(CN(Cc2cccc2)S(=O)(=O)c2ccc(C(=O)O)cc2)c(OC)c1</chem>	10760	1076	8773	0.0000	4.9681
CHEMBL394 6036	<chem>O=C(O)C1CCC(CN(Cc2ccc(F)cc2)S(=O)(=O)c2cccc2)CC1</chem>	240	0024	8876	0.0000	6.6197
CHEMBL389 5732	<chem>CCCOc1ccc(CN(Cc2ccco2)S(=O)(=O)c2ccc(C(=O)O)cc2)cc1</chem>	2500	025	5999	0.0000	5.6020

Appendix

CHEMBL309 2287	<chem>COc1ccc(CN(Cc2ccccc2)S(=O)(=O)c2ccc(C(=O)O)cc2)cc1</chem>	220	0022	6.6575 7732
CHEMBL390 2385	<chem>CCc1ccc(CN(CC2CCC(C(=O)O)CC2)C(=S)Nc2c cccc2C)cc1</chem>	5018	05018	5.2994 6934
CHEMBL396 7689	<chem>CCOC(=O)C1CCC(CN(Cc2ccccc2Cl)S(=O)(=O)c 2ccc(C)cc2)CC1</chem>	2816	02816	5.5503 6735
CHEMBL135 6858	<chem>CCOC(=O)C1CCC(CN(Cc2ccccc2)S(=O)(=O)c2c cc(Cl)cc2)CC1</chem>	672	00672	6.1726 3073
CHEMBL108 2389	<chem>O=C(O)c1ccc(CN(Cc2ccccc2)S(=O)(=O)c2ccc(Cl)cc2)cc1</chem>	394	00394	6.4045 0378
CHEMBL397 0999	<chem>Cc1ccccc1CN(Cc1ccccc1)S(=O)(=O)c1ccc(C(=O) O)cc1</chem>	2926	02926	5.5337 2568
CHEMBL390 7785	<chem>Cc1ccc(S(=O)(=O)N(Cc2ccc(F)cc2)Cc2ccc(C(=O))O)cc2)cc1</chem>	54	00054	7.2676 0624
CHEMBL397 1645	<chem>COc1ccc(CN(Cc2ccccc2C)S(=O)(=O)c2ccc(C(=O))O)cc2)cc1</chem>	5316	05316	5.2744 1503
CHEMBL392 3737	<chem>COc1ccccc1CN(Cc1ccco1)S(=O)(=O)c1ccc(C(=O))O)cc1</chem>	12000	12	4.9208 1875
CHEMBL389 5068	<chem>Cc1ccc(S(=O)(=O)N(Cc2ccccc2)CC2CCC(C(=O) O)CC2)cc1</chem>	14	00014	7.8538 7196
CHEMBL132 3541	<chem>COc1ccc(CN(CC2CCC(C(=O)O)CC2)C(=S)Nc2c cc(C)c(Cl)c2)cc1</chem>	6136	06136	5.2121 1465
CHEMBL396 5603	<chem>Cn1c(=O)c2c(SCC(=O)NCc3ccccc3)ccnc2n(C)c1 =O</chem>	710	0071	6.1487 4165
CHEMBL389 4540	<chem>COc1ccc(CN(Cc2ccco2)S(=O)(=O)c2ccc(C(=O)O)cc2)cc1</chem>	590	0059	6.2291 4799
CHEMBL390 1193	<chem>COc1cccc(CN(Cc2ccco2)S(=O)(=O)c2ccc(C(=O) O)cc2)c1</chem>	10000	1	0.0000 5